Energy 308 (2024) 132878

Contents lists available at ScienceDirect

Energy

journal homepage: www.elsevier.com/locate/energy

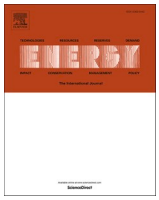

An optimal load distribution and real-time control strategy for integrated energy system based on nonlinear model predictive control

Jiarui Li [a,1], Zhiwei Jiang [a,1], Yuan Zhao [b], Xiaolu Feng [a], Menglian Zheng [a,c,*]

[a] Institute of Thermal Science and Power Systems, School of Energy Engineering, Zhejiang University, Hangzhou, 310027, China
[b] Power China Huadong Engineering Corporation Limited, Hangzhou, 311122, China
[c] State Key Laboratory of Clean Energy Utilization, Zhejiang University, Hangzhou, 310027, China

ARTICLE INFO

Keywords:
Integrated energy system
Model predictive control
Optimal load distribution
Real-time control
System identification
Varying operational conditions

ABSTRACT

Efficient operational scheduling and control are vital for the operation process of the Integrated Energy System (IES), especially under varying operational conditions. An optimal load distribution and real-time control strategy for IES based on Nonlinear Model Predictive Control has been developed to synergistically improve equipment output performance and reduce operating costs. In the proposed strategy, the IES model that integrates linear parameter-varying models for devices and dynamic models for pipe networks, has been constructed via system identification methodology under varying operational conditions. Thus, a hierarchical operation and control framework is established using the model predictive control strategy, including real-time prediction objective, optimal load distribution objective, and optimization algorithms. Consequently, a case study is performed to investigate the supply-demand balance and economic benefit of the proposed strategy. From the aspect of supply-demand balance, the average energy supply-demand discrepancy by using the proposed strategy (for cooling and heating) is approximately 25 %~33 % that under the steady-state strategy. By means of the proposed strategy, an outstanding equipment output performance will be achieved and supply-demand discrepancy can be dramatically reduced. From the perspective of economic performance, the proposed strategy, which fully considers the nonlinearity of devices, exhibits a 16 % decrease in the operational cost compared to that under the linear dynamic strategy. Through the proposed strategy, efficiency losses are expected to degrade with an excellent economic benefit. Therefore, the suggested strategy is promising and suitable for varying operational condition scenarios.

Nomenclature

Symbols			
T	Time	ET	Average time
G	Transfer function	G	Transfer function
v	Gas valve opening	ele	Electricity output
V	Laplace transform of v	ELE	Laplace transform of ele
$heat$	Heating output	$cold$	Cooling output
$HEAT$	Laplace transform of $heat$	$CLOD$	Laplace transform of $cold$
a	Damper angle of induced draft fan	A	Laplace transform of a
p	Laplace transform of ele	P	Probability of a certain event
α	Weight coefficient	ω	Scheduling variable
R	Operation and maintenance cost	C	Price
u	Input value	J	Objective function
Ts	Sampling time	q	Waste heat
Superscripts and subscripts			
gt	Gas turbine	gb	Gas boiler
ec	Electric chiller	ac	Absorption chiller
b	Waste heat boiler	h	High
heat_grid	Heating network	cold_grid	Cooling network
l	Low	m	Medium
sw	Switching time	min	Minimum
ex	Exhust out of gas turbine	ex_b	Exhust sent into waste heat boiler
ex_ac	Exhust sent into absorption chiller	sys	System
Abbreviations			
IES	Intergrated energy system	MPC	Model predictive control

(*continued on next column*)

(*continued*)

(*continued on next page*)

* Corresponding author. Institute of Thermal Science and Power Systems, School of Energy Engineering, Zhejiang University, Hangzhou, 310027, China.
E-mail address: menglian_zheng@zju.edu.cn (M. Zheng).
[1] Co-first authors.

https://doi.org/10.1016/j.energy.2024.132878
Received 17 March 2024; Received in revised form 29 May 2024; Accepted 18 August 2024
Available online 22 August 2024

(*continued*)

SQP	Sequential quadratic programming	LPV	Linear parameter-varying
NMPC	Nonlinear model predictive control	GBN	Gaussian binary noise
O&M	Operation and maintenance		

1. Introduction

The issues of fossil energy resource depletion and environmental pollution have become increasingly critical, promoting a trend toward a clean, low-carbon energy structure. Consequently, the Integrated Energy System (IES), in which multiple heterogenous energy sources are interconnected, converted, and complemented, has become a focal point of interest in the energy field [1]. Notably, IES exhibits a closer proximity to end-users, resulting in a higher load response level than conventional energy systems [2]. Additionally, under varying operational conditions, the operation of IES is characterized by complex dynamic nonlinearity attributable to the large inertia and long-term delays associated with the equipment and heat and mass transfer processes [3]. These present challenges for real-time multi-energy flow balance and dynamic trajectory tracking control for multiple equipment within the IES. Hence, implementing efficient operational scheduling and control is critical for meeting the real-time demands in multiple energy carriers, mitigating the deviation between actual energy distribution and the planned schedule and facilitating the complementarity of diverse energy sources.

A large and growing body of literature has investigated the optimal scheduling of IES, which is a complex decision problem considering factors such as equipment operation, multiple heterogeneous energy coupling constraints, and various demands. To improve the flexibility of interactions between IES and the energy supply network, a number of studies have been conducted to involve a wide range of stakeholders and energy carriers into the IES systems. For example, Yu et al. [4] proposed a bi-level scheduling strategy for IES to optimize the integrated demand response mechanism and the reasonable energy storage capacity. Basu et al. [5] investigated a dynamic dispatch model considering clean water, methane, electricity, and heat demands and discussed the influence of optimum dispatch results on the total cost. Bu et al. [6] established a low-carbon economic dispatch model considering integrated demand response in an energy park where the electricity–hydrogen–gas energy systems are integrated with carbon capture equipment. Combined with electricity, heat, gas, and carbon coupling characteristics, Wang et al. [7] built a low-carbon economic dispatch modal to reduce the carbon emission of IES. Currently, most relevant research [8–10] primarily focuses on achieving scheduling objectives, followed by controlling IES using optimized results. This approach mainly addresses open-loop optimization problems and lacks the control or adjustment of scheduling objectives based on feedback.

Model Predictive Control (MPC), as an efficient operational optimization and control approach based on rolling optimization and feedback correction, is capable of addressing the operation complexity and unpredictability arising from the dynamic nonlinearity of IES. Yao et al. [11] developed a multi-level MPC-based optimization model for IES, which is composed of an intra-day optimization and real-time optimization, using predicted data of renewable energy and load as inputs based on machine learning. Zhao et al. [12] designed a two-stage stochastic-MPC dispatch strategy for integrated power and natural gas systems, wherein data-driven chance constraints for the dispatch plan were proposed to prevent the adverse effects of stochastic prediction errors. Similarly, several references [13–17] effectually applied one-stage or two-stage MPC to improve the operation of IES with consideration of the stochasticity of renewable power and load. Wei et al. [18] devised an improved stochastic-MPC strategy of IES based on a single-layer multi-timescale framework and assessed the economic, robustness, and computational efficiency performance of the proposed strategy by comparing to those under a traditional single-layer strategy and those under a hierarchical strategy. Besides, the application of muti-timescale frameworks has also been explored in IES [19–21]. Zhu et al. [22] put forward a unified MPC-based control strategy for a coal-fired plant integrated with battery energy storage systems, wherein the fuzzy logic-based MPC was employed to cope with the large nonlinearity of the boiler and the turbine units. Previous studies[23,24] also proposed MPC-based approaches of IES for enhanced synergy and demand response. Lv et al. [25] built MPC-based robust scheduling for communal IES, consisting of rolling optimization and robust constraint generation, and they conducted a case study by linearizing nonlinear terms in the model. Currently, much research on the MPC-based operational optimization and control method of IES is primarily centered on enhancing system operational flexibility, mainly including addressing scheduling issues considering uncertainties from forecasting data (renewable power and load), utilizing muti-timescale framework, and improving management of energy supply process and so on. However, the research mainly pertains to linear system models and models with nonlinear terms, with limited attention given to the exploration of Nonlinear Model Predictive Control (NMPC) for nonlinear IES system models.

During NMPC algorithms, integrating nonlinear model predictions and nonlinear constraints into the optimization problem is essential, but it can greatly increase computation complexity. The LPV model is recognized as a promising alternative to model processes with complex dynamics, which are linear in the state space while nonlinear in the parameter space [26]. Therefore, the available LPV-MPC model can be solved by a sequential QP-based solution, which is roughly equivalent to modern NMPC solvers in terms of computational performance [27]. LPV model structure can be broadly classified into two categories: parametric structure and multiple model structure. Considering model stability, the LPV models with multiple model structures are more suitable for describing energy systems, which involve a wide range of energy carriers. The recent literature concerning the LPV-MPC model focuses on the application of the LPV-based state observer, the operational optimization of a specific device within the energy system, and the operational optimization of the energy systems. Both [28,29] effectually applied the LPV-based state observer to estimate faults that occur in the energy system, which can effectively enhance the control performance of MPC. Besides, as detailed in Refs. [30–32], the LPV-based model with the parametric structure was utilized to address the complex mechanistic modeling of specific devices in the MPC framework. In previous work, the LPV-MPC models related to the operational optimization of the energy system have been explored. Ji et al. [33] developed a data-driven quasi-LPV model with the parametric structure of an organic Rankine cycle system. The corresponding MPC algorithm via quasi-LPV representation was established to realize prediction accuracy improvement. Shi et al. [34] applied the LPV-based model with the multiple model structure to build the multiple-input single-output model of the circulation fluidized bed boiler, and its effectiveness was validated. However, far too little attention has been paid to efficiently building the multiple-input multiple-output (MIMO) model of IES via the LPV models with the multiple model structure in the MPC framework.

This prospective study presents an NMPC-based optimal load distribution and real-time control strategy for IES, considering dynamic nonlinearity under varying operational condition. The specific contributions of this research are as follows.

(1) By means of integrating the LPV model with the multiple model structure into the MPC framework, the proposed NMPC strategy takes into account the nonlinear dynamic characteristics of the IES while ensuring model stability and alleviating the computational burden. This work would make a rather practical engineering contribution to the field of IES modeling.
(2) The introduced approach accounts for the dynamic characteristics of the cooling process, heating process, and equipment under varying operational condition, which in turn leads to a reduction

in the supply-demand deviation derived from model-schedules mismatch, ultimately resulting in an enhanced level of equipment output performance.

(3) This approach fully considers the nonlinearity of IES operation under varying operational conditions, which can enable accurate modeling of input-output relationships of devices and successfully preventing untimely equipment output, aiming at reducing efficiency losses and improving the economic performance.

2. System description

2.1. Reference load data

To introduce the proposed NMPC-based optimal load distribution and real-time control strategy and assess its performance, the reference hourly cooling, heating, and electric load data for one year within a specific building area at the Tempo campus of Arizona State University in the United States has been selected for the case study [35], as visually depicted in Fig. 1. Furthermore, the cooling consumption is calculated based on the temperature difference and flow rate of air and chilled water. Similarly, the load data of heating is determined by the temperature difference and flow rate of air and hot water. And electric consumption is measured through the electrical meters of the building.

2.2. Integrated energy system

The schematic diagram of IES and energy flows is illustrated in Fig. 2, which intuitively provides multi-energy conversion among devices. Besides, the IES is comprised of the gas turbine, waste heat boiler, absorption chiller, gas boiler, electric chiller, heating network, cooling network, and power grid.

The natural gas can be combusted to form hot flue gas in the gas turbine that drives the rotor of the electric generator for power generation. In situations where the power supplied by the gas turbine is insufficient, power supplementation to end users is carried out by the power grid. Afterward, exhaust gas yielded from the gas turbine is delivered to the absorption chiller and waste heat boiler, respectively, to recover thermal energy. These cooling and thermal energy are then distributed to end users through cooling and heating networks. In instances where insufficient cooling energy is provided by the absorption chiller, additional cooling energy can be supplied by the electric chiller powered by the power grid, satisfying users' cooling demands. When thermal energy derived from the waste heat boiler is insufficient, natural gas is burned to supplement the thermal energy via the gas turbine, meeting end users' demands for heating and hot water.

3. Modeling of integrated energy system operation

3.1. System identification methodology under varying operational conditions

The methodology of system identification under varying operational conditions is displayed in Fig. 3. In general, a complete system identification process should include four steps: identification experiment design, model structure selection, parameter estimation, and model validation [36]. The proposed IES can be mathematically established as the MIMO dynamic nonlinear model in accordance with system identification methodology. Prior to system identification, the dynamic modules were constructed for each operational device and the cooling and heating networks within the APROS software platform. By utilizing system identification methodology, step response tests were first conducted on device models and network models to collect relevant data (for example, step response time and nonlinear characteristics). Subsequently, based on the actual operational conditions of each device, the

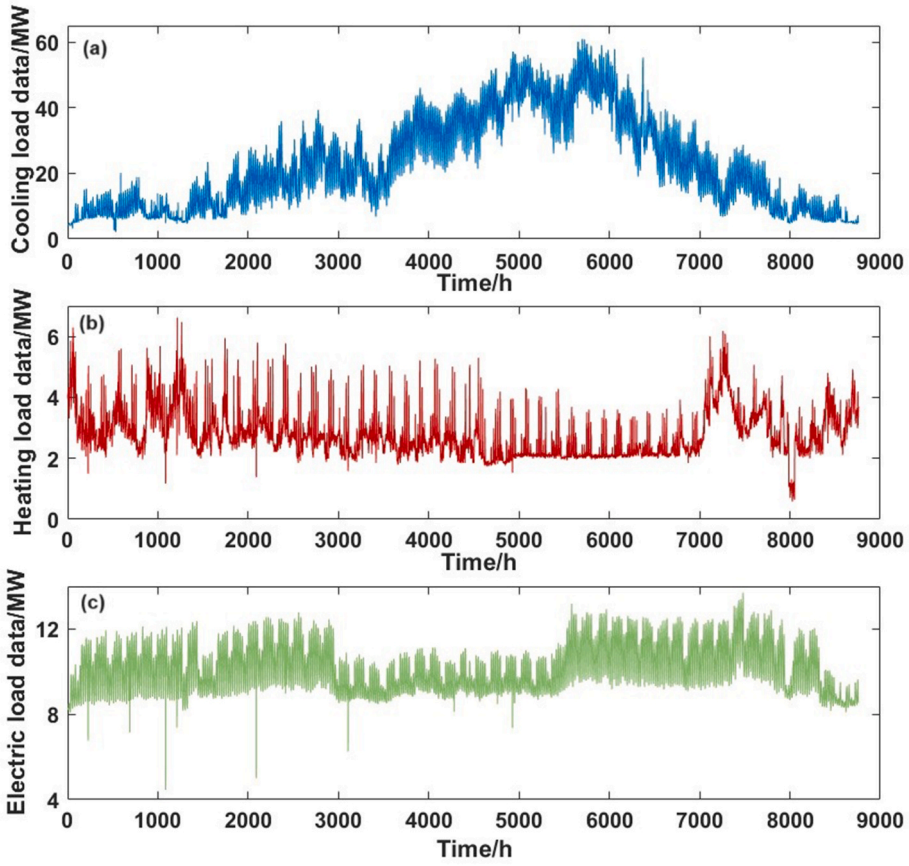

Fig. 1. (a) Hourly cooling load profile for one year. (b) Hourly heating load profile for one year. (c) Hourly electric load profile for one year.

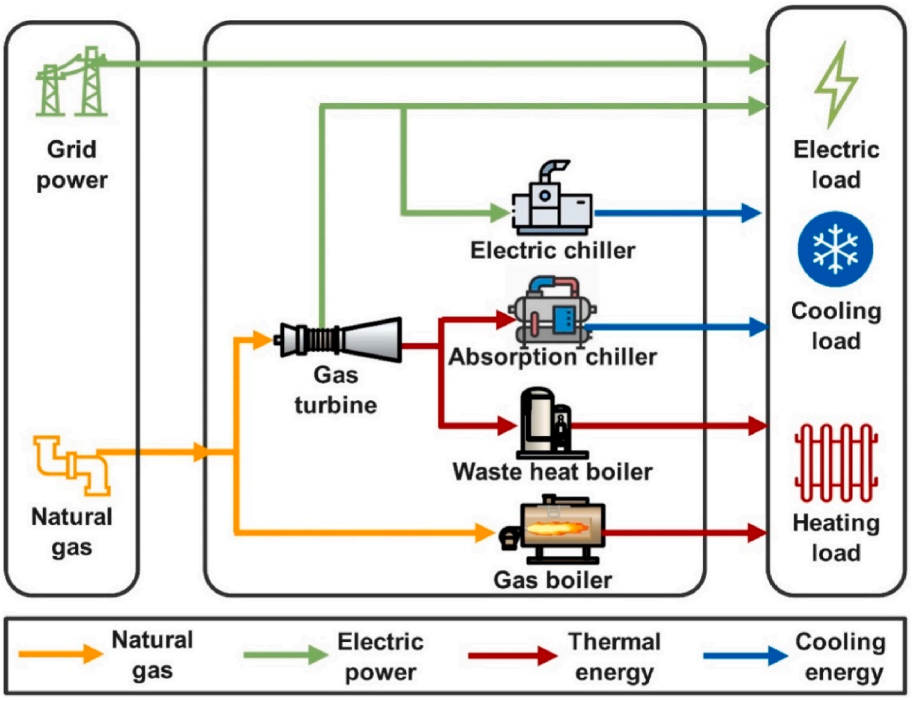

Fig. 2. Schematic diagram of IES and energy flows.

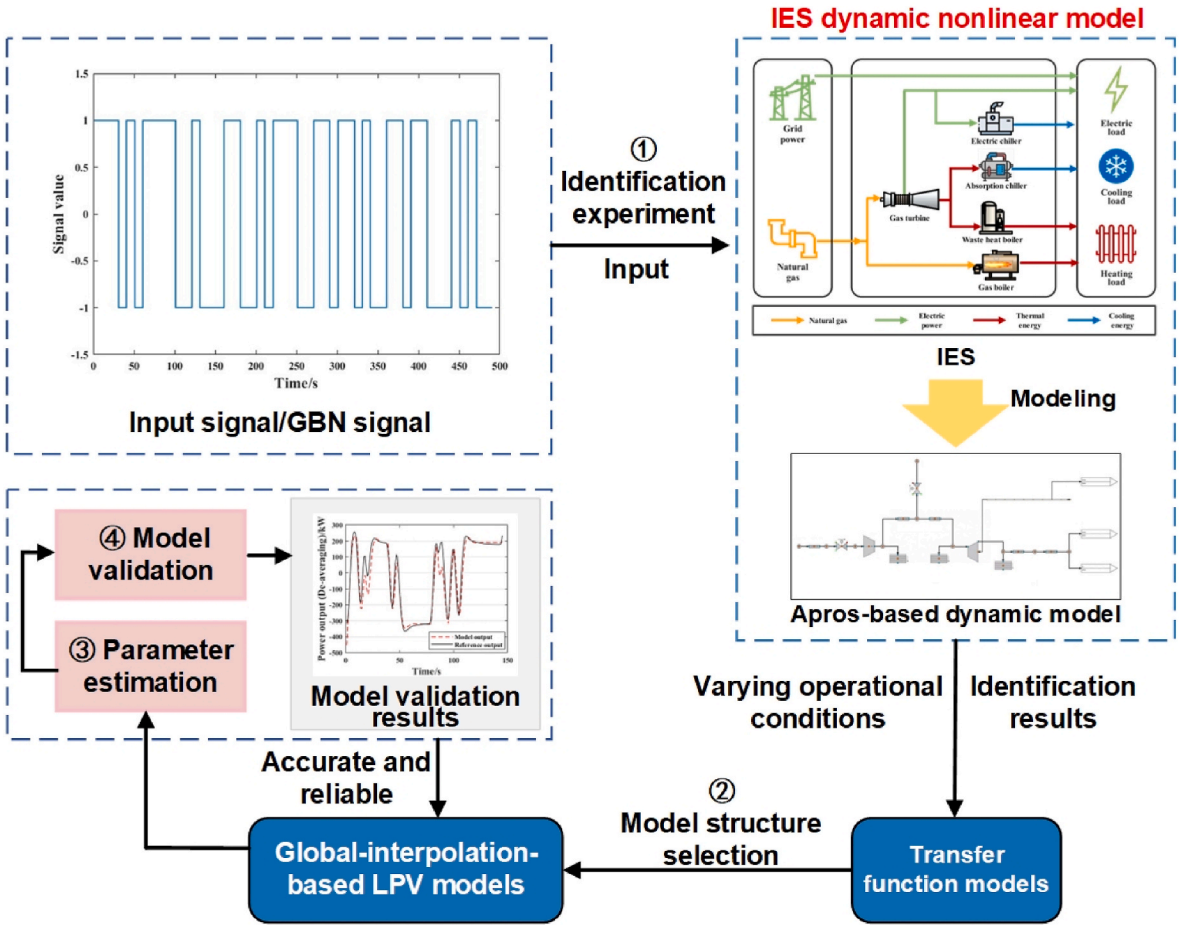

Fig. 3. The methodology of system identification.

variable weighting coefficients, which were determined by scheduling parameter (for instance, power output) via the linear interpolation method, were applied to combine the system-identification device models under different operational conditions, resulting in the formulation of Linear Parameter-varying (LPV) model for each device under all operational conditions. According to the compositional structure of the IES, an overarching MIMO model (dynamic nonlinear model) for the IES was implemented by considering the interrelationships among the various operational devices and networks.

To obtain an accurate and reliable IES dynamic nonlinear model under varying operational conditions, an adaptive Gaussian Binary Noise (GBN) signal is employed as the identification excitation signal in the identification experiment, and Fig. 4 (a) illustrates a GBN signal. The GBN signal switches between values within the range of -a and a (as shown in Fig. 4 (a), with a set to 1), and at each switching instant t, the transformation follows the rules defined in Equation (1). In this equation, P represents the probability of a certain event, and p_{sw} is the switching probability.

$$\begin{aligned} P[u(t) = -u(t-1)] &= p_{sw} \\ P[u(t) = u(t-1)] &= 1 - p_{sw} \end{aligned} \tag{1}$$

Further, in order to avoid the effects of unmeasurable disturbances and ensure the acquisition of adequate input-output data, it is essential to design appropriate signal excitation time and average switching time. The minimum dwell time, denoted as $T_{\min}$, is defined as the duration for which the GBN signal remains at a constant level. The switching time, denoted as T_{sw}, refers to the time interval between two consecutive transitions. The average switching time ET_{sw} can be computed using Equation (2). The average switching time is determined to be 10 s, as introduced in Fig. 4 (a).

$$ET_{sw} = \frac{T_{\min}}{p_{sw}} \tag{2}$$

Typically, the excitation time can be selected as 6–18 times the open-loop step response time of the process. Furthermore, the average switching time of the excitation signal can be designed following the principle described in Equation (3) [36].

$$ET_{sw} = \frac{98\% * step\ response\ time}{3} \tag{3}$$

3.2. System-identification-based equipment model

Based on the APROS simulation software, a dynamic nonlinear model of the proposed IES structure was established, as shown in Appendix A. System identification methods are employed to construct dynamic transfer models for each equipment under different operational conditions. Then, the time-varying operation condition parameter, in particular the operation condition intensity, is specified as the scheduling variable that is used to parameterize the LPV model. More illustration about the verifications between actual values and simulation results has been provided in supplementary material.

Taking the modeling of the gas turbine equipment as an example, a

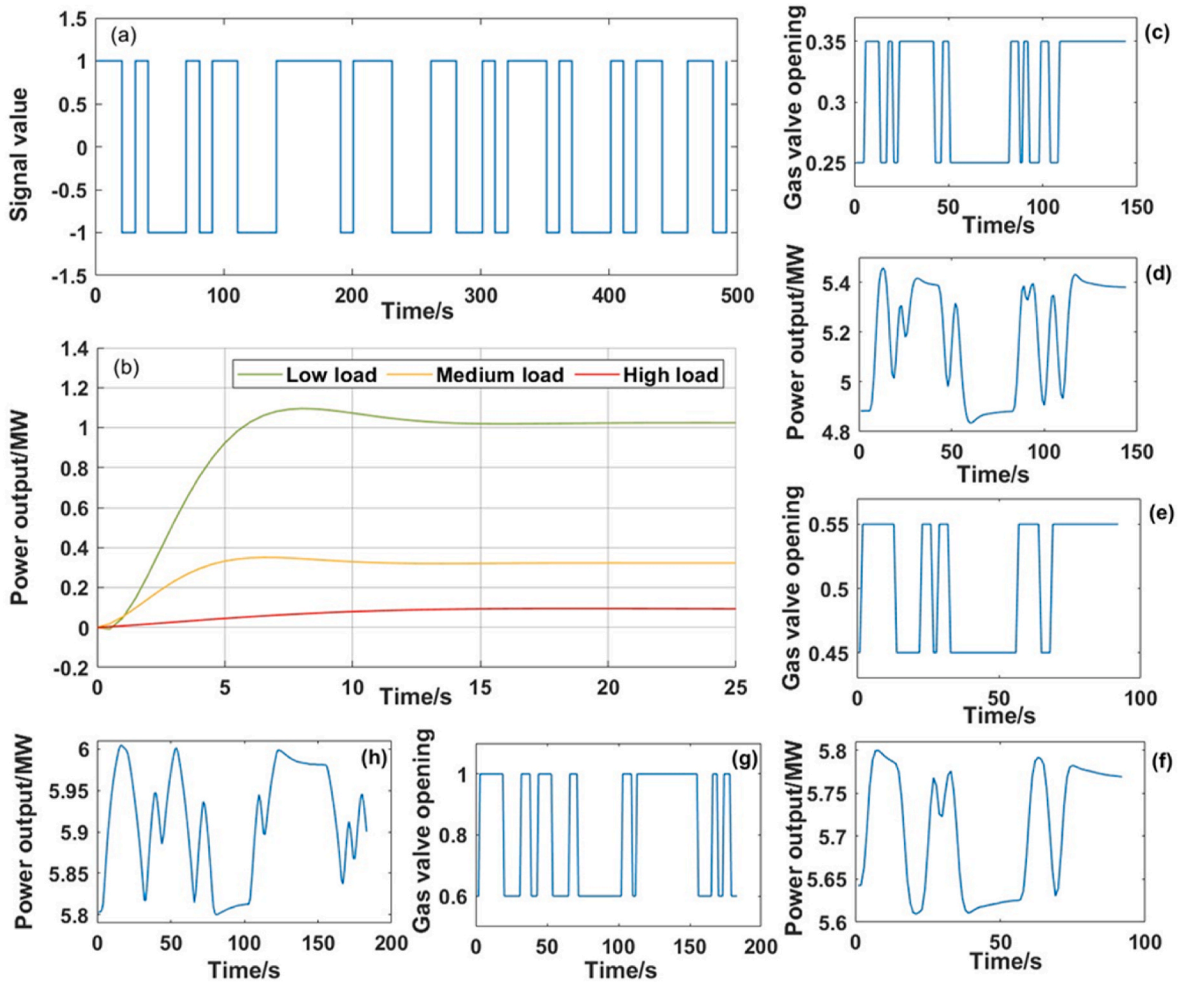

Fig. 4. (a) Diagram of GBN signal. (b) Results of step response tests for the gas turbine. (c) Input signal under low-load operation condition. (d) Output signal under low-load operation condition. (e) Input signal under medium-load operation condition. (f) Output signal under medium-load operation condition. (g) Input signal under high-load operation condition. (h) Output signal under high-load operation condition.

gas turbine model is developed using the APROS dynamic simulation software, as shown in Figure A1. The input and output variables for the gas turbine model are the extent of the valve opening and the gas turbine's power output. At the low-load, medium-load, and high-load operational conditions, step response tests were conducted on the gas turbine model by setting input signals of the extent of valve opening to 0.2. The results of step response tests are shown in Fig. 4 (b), with the corresponding gas turbine power outputs for low, medium, and high loads being 5200 kW, 5600 kW, and 5900 kW, respectively. The step response results reveal a certain level of nonlinearity in the operational characteristics of the gas turbine under varying operational conditions.

Based on the principle defined by Equation (3), the identification experiments at low, medium, and high load operational conditions are initially designed with selecting the power output of the gas turbine as a scheduling parameter. The corresponding excitation input (deemed as a GBN signal) and the output signals obtained from the APROS simulation system are shown from Fig. 4 (c) to Fig. 4 (h). At low, medium and high load operational conditions, the identified transfer function models are denoted as G_{gt_l}, G_{gt_m} and G_{gt_h}, respectively, as shown in Equation (4). The results of model accuracy verification are presented from Fig. 5 (a) to Fig. 5 (c).

$$\begin{aligned} G_{gt\_l} &= \frac{-475.4\,s + 1437}{s^2 + 0.6868\,s + 0.2807} \\ G_{gt\_m} &= \frac{84.5\,s + 542.4}{s^2 + 0.7218\,s + 0.3462} \\ G_{gt\_h} &= \frac{35.36\,s + 20.45}{s^2 + 0.3025\,s + 0.04511} \end{aligned} \tag{4}$$

By utilizing the model structure depicted in Equation (5), a global-interpolation-based LPV model was constructed to obtain the gas turbine model under varying operational conditions:

$$ELE_{gt} = \alpha_{gt\_l}(\omega_{gt})G_{gt\_l}V_{gt} + \alpha_{gt\_m}(\omega_{gt})G_{gt\_m}V_{gt} + \alpha_{gt\_h}(\omega_{gt})G_{gt\_h}V_{gt} \tag{5}$$

Where V_{gt} represents the input variable, corresponding to the Laplace transform of the extent of the valve opening; ELE_{gt} represents the output variable, corresponding to the Laplace transform of the gas turbine power output; $\alpha_{gt\_l}(\omega_{gt})$, $\alpha_{gt\_m}(\omega_{gt})$ and $\alpha_{gt\_h}(\omega_{gt})$ are the variable weight coefficients for the models at different operational conditions; ω_{gt} represents the scheduling parameter (the power output of gas turbine).

The global-interpolation-based LPV model of the gas turbine is established by using piecewise linear functions to describe its weight coefficients, which are given in Equation (6). The accuracy of the LPV model of the gas turbine is evaluated by comparing the input-output data (at a specific operational condition) of the gas turbine model constructed in APROS with the LPV model of the gas turbine. The results of this comparison are presented in Fig. 5 (d). The remaining equipment is modeled using the same approach to construct LPV models (details can be found in supplementary material).

$$\alpha_{gt\_l}(\omega_{gt}) = \begin{cases} 1 & \omega_{gt} \le 5200\text{kW} \\ \dfrac{5700 - \omega_{gt}}{5700 - 5200} & 5200\text{kW} < \omega_{gt} < 5700\text{kW} \\ 0 & \omega_{gt} \ge 5700\text{kW} \end{cases}$$

$$\alpha_{gt\_m}(\omega_{gt}) = \begin{cases} 0 & \omega_{gt} \le 5200\text{kW} \\ \dfrac{\omega_{gt} - 5200}{5700 - 5200} & 5200\text{kW} < \omega_{gt} < 5700\text{kW} \\ \dfrac{5900 - \omega_{gt}}{5900 - 5700} & 5700\text{kW} \le \omega_{gt} < 5900\text{kW} \\ 0 & \omega_{gt} \ge 5900kW \end{cases} \tag{6}$$

$$\alpha_{gt\_h}(\omega_{gt}) = \begin{cases} 0 & \omega_{gt} \le 5700kW \\ \dfrac{\omega_{gt} - 5700}{5900 - 5700} & 5700\text{kW} < \omega_{gt} < 5900\text{kW} \\ 1 & \omega_{gt} \ge 5900kW \end{cases}$$

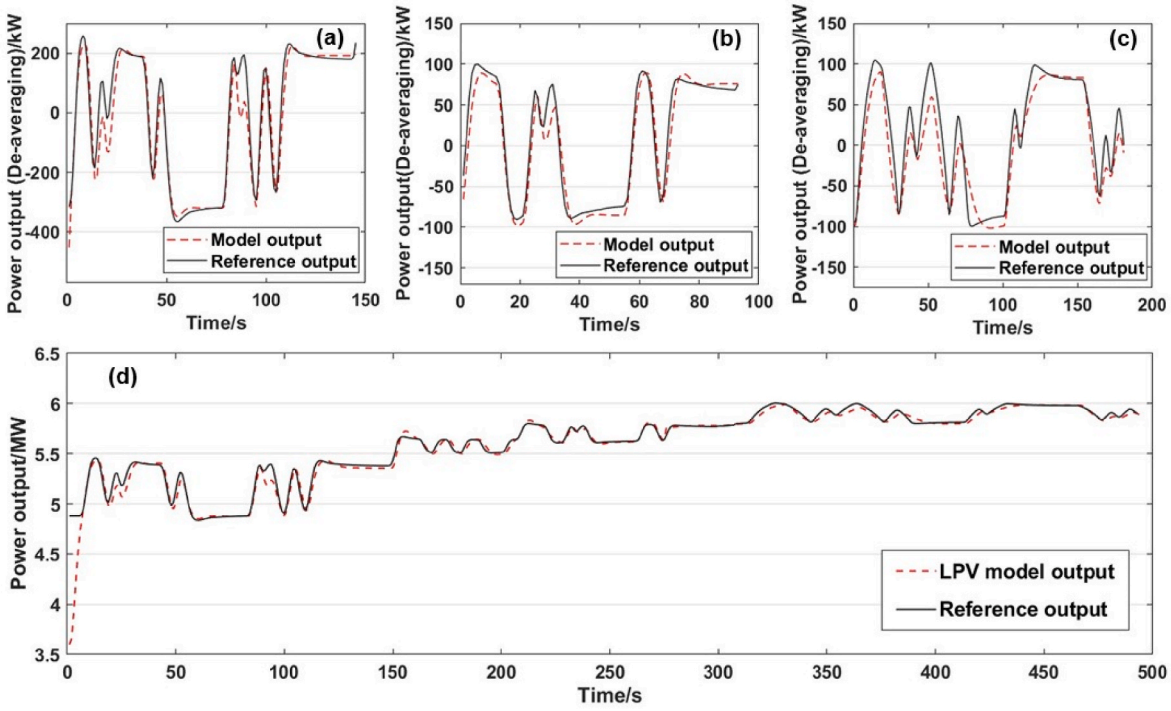

Fig. 5. (a) Model validation results (mean-subtraction) of gas turbine under low-load operation condition. (b) Model validation results (mean-subtraction) of gas turbine under medium-load operation condition. (c) Model validation results (mean-subtraction) of gas turbine under high-load operation condition. (d) LPV model validation of gas turbine (Reference data is derived from APROS-based model output).

3.3. System-identification-based pipe network model

In this study, the pipe networks (heating network and cooling network) are divided into primary and secondary networks. The drain water out of the primary network is preheated through the heat exchange at the heat source and then it (as feedwater at the primary network) is distributed into various heat exchange stations, where thermal energy existing in feedwater is supplied for drain water (at the secondary network). As a result, the feedwater at the secondary network can play a critical role in satisfying the heating and cooling demand. The basic structure of the pipeline network is depicted in Fig. 6 (a).

Based on the fundamental structure of the pipeline network, a pipeline network simulation system is constructed in APROS. Figure A6 (a) illustrates the simulation system for the primary side of the cooling and heating networks (both adopting the same structural format), while Figure A6 (b) represents the simulation system for the secondary network connected to a specific heat exchange station.

The pipeline network simulation system is subjected to step response testing, and the results are depicted in Fig. 6 (b) and 6 (c). The outcomes of the step response test indicate that the dynamic response time of the pipeline network model is significantly greater compared with that of the individual cooling or heating equipment. The inertia of the energy supply process (within IES) is primarily determined by the dynamic response time of the pipeline networks. Hence, considering the dynamic characteristics of the pipeline network is essential.

During the identification experiments of the pipe network model, the input variables of the pipe networks are adjusted by varying the cooling and heating outputs at different cooling and heating sources. Furthermore, the corresponding output variables are collected, and the input-output signals are shown from Fig. 6 (d) to Fig. 6 (g). The identified transfer functions (for the heating network and cooling network) are formulated as G_{heat_grid} and G_{cold_grid} via the method mentioned in Section 3.1, as shown in Equation (7). Fig. 6 (h) and 6 (i) illustrate the outputs of network models (for the cooling network and heating network) are quite similar to the reference data (introduced in Section 2.1), thereby the network models are accurate and credible.

$$G_{heat\_grid} = \frac{0.001399\,s + 2.83\mathrm{e}-06}{s^2 + 0.007885\,s + 2.895\mathrm{e}-06}$$
$$G_{cold\_grid} = \frac{2.201\mathrm{e}-05}{s^2 + 0.03105\,s + 2.21\mathrm{e}-05} \quad (7)$$

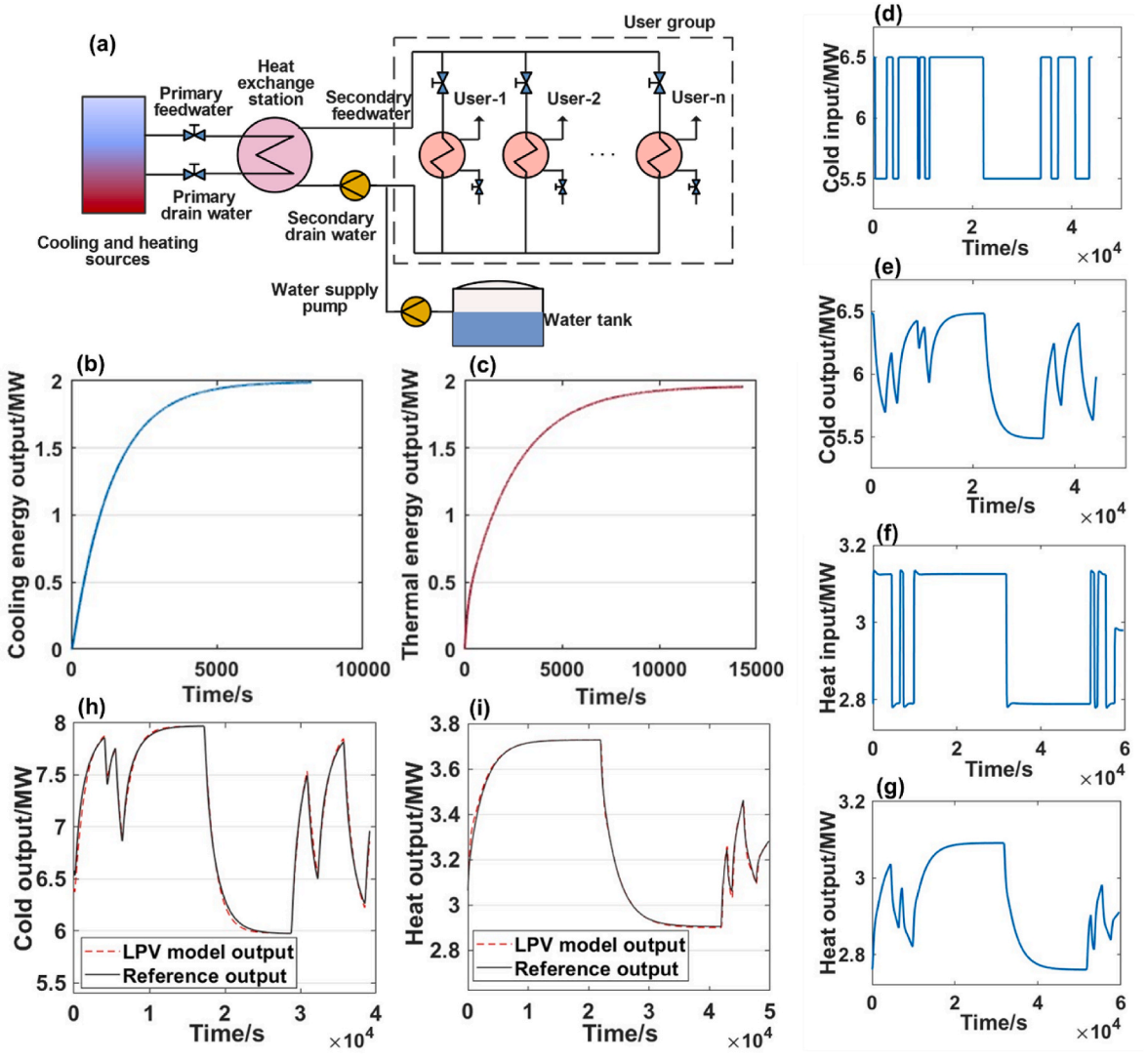

Fig. 6. (a) Fundamental structure of pipe network. (b) Results of step response test for cooling pipe network with an input step size of 2000 kW. (c) Results of step response test for heating pipe network with an input step size of 2000 kW. (d) Input signal of cooling pipe network model. (e) Output signal of cooling pipe network model. (f) Input signal of heating pipe network model. (g) Output signal of heating pipe network model. (h) Model validation of cooling pipe network. (i) Model validation of heating pipe network.

4. Optimal load distribution and real-time control strategy based on NMPC

To enhance the load response process of IES, a conceptual NMPC-based strategy incorporating optimal load distribution and real-time control has been put forward, as sketched in Fig. 7. Compared with conventional economic MPC, the prediction model of MPC in this study was constructed by integrating with the IES model under varying operational conditions through LPV embedding. Thus, the "device nonlinear dynamic information" of the IES is included in the MPC prediction results. The proposed strategy aims to facilitate the best energy supply-demand matching and timely adjusting the electric, heating, and cooling output (for the IES dynamic nonlinear model), which includes real-time prediction objective (for the prediction domain), optimal load distribution objective (for the control domain), and optimization algorithm. Given that short-term load fluctuations are not considered, the strategy presented in this paper does not incorporate a disturbance model. Subsequently, the essential components of the designed strategy are further elaborated in-depth.

4.1. Real-time prediction objective

Fig. 8 illustrates the optimization principle of the MPC optimization principle. At a certain time instant k, based on the measured current output $y(k)$ of the system and the reference output r, a rational scheme is devised for the inputs z over the future p time instants (p is also referred to as the prediction horizon). Therefore, the deviation between the predicted output y_p and the reference output r is minimized as much as possible in the forthcoming p time instants. Due to the inherent dynamic discrepancies between the IES model and the actual system, the optimal inputs, as determined by the planning, are usually executed only up to the time instant k+1. According to the latest output of the IES model (at k+1 time), an updated input planning is performed. This iterative process ensures continuous forward-rolling optimization within the time horizon. In this study, the reference output r corresponds to the reference cooling, heating, and electric loads (as provided in Fig. 1), which are known along the future system trajectories. The output y represents the output of the IES in terms of cooling, heating, and electric supply. The input z corresponds to the input variables of various cooling, heating, and electric supply equipment, which is instantaneously determined by the MPC at each sample.

The real-time predictive objective is commonly described using state-space representation in accordance with the MPC optimization principle, as shown in Equation (8), where $x(k)$ denotes the state variables of the system at time instant k.

$$\begin{aligned} x(k+1) &= f(x(k), z(k)) \\ y(k) &= h(x(k), z(k)) \end{aligned} \tag{8}$$

At time instant k, the current initial state of the system $x(k)$ and the output $y(k)$ value can be measured. Using the input variable sequence Z_k obtained from planning, the output sequence Y_k within the prediction horizon can be computed using the IES model. Z_k and Y_k can be expressed as follows:

$$Z_k = \{z(k|k), z(k+1|k), \cdots, z(k+p-1|k)\} \tag{9}$$

$$Y_k = \{y(k+1|k), y(k+2|k), \cdots, y(k+p|k)\} \tag{10}$$

Where $k+i|k$ represents the predicted value at time instant $k+i$, based on the information available at time instant k.

Furthermore, to make the predicted output closely track the reference output r, Equation (11) is employed to describe the degree of tracking. The real-time prediction objective J_y indicates that the optimized predicted system outputs are closer to the reference data, implying better real-time control performance of the system.

$$J_y(Z_k) = \sum_{j=1}^{n_y} \sum_{i=1}^{p} \left\{ w_{i,j}^{y} \left[r_j(k+i\,|k) - y_j(k+i\,|k) \right] \right\}^2 \tag{11}$$

Where k represents the current scheduling time instant; p denotes the prediction horizon; n_y represents the number of output variables; $r_j(k+i|k)$ denotes the predicted values of the jth reference outputs at time instant $k+i$, based on the information available at time instant k; $y_j(k+i|k)$ denotes the predicted values of the jth system outputs at time instant $k+i$, based on the information available at time instant k; and $w_{i,j}^{y}$ represents the weight coefficient of the jth output at time instant $k+i$.

4.2. Optimal load distribution objective

Due to the multi-energy coupling characteristics inherent in IES, it

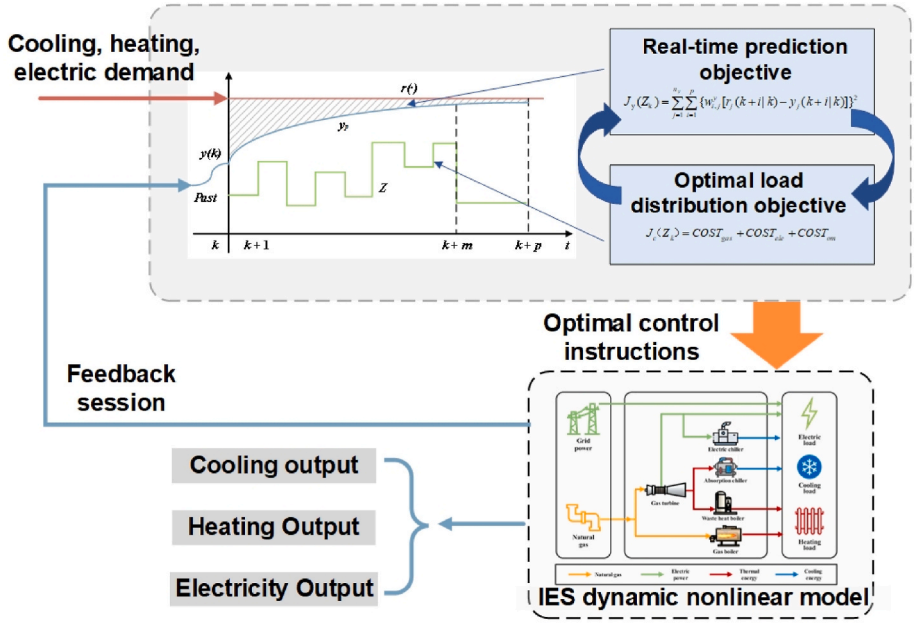

Fig. 7. Diagram of NMPC-based optimal load distribution and real-time control strategy.

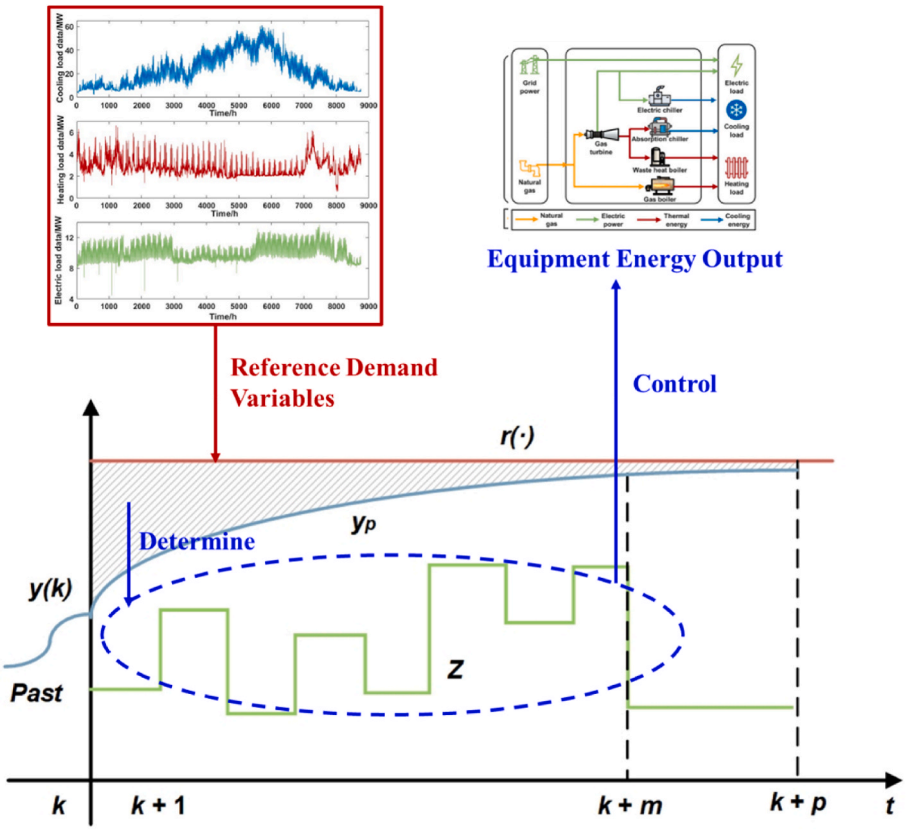

Fig. 8. Diagram of MPC optimization principle.

exhibits multiple load distribution schemes, which generally result in comparable operational benefits. To identify the optimal load distribution strategy, an optimal load distribution objective function involving natural gas cost, grid electricity cost, and operation and maintenance (O&M) cost has been formulated, as described as Equation (12). In the future, a carbon emission penalty factor could be added to the optimal load distribution objective function to improve the sustainability of the plant (i.e., minimizing the use of natural gas for electrical demand).

$$J_c(Z_k) = COS\,T_{\text{gas}} + COS\,T_{\text{ele}} + COS\,T_{\text{om}}$$

$$= \sum_{i=1}^{p} \left[\left(gas_{gt\_i} + gas_{gb\_i}\right) * Ts/\rho_{\text{gas}} * C_{\text{gas}} + \left(ele_{ec\_i} + ele_{grid\_i}\right) * Ts * R_{ele\_i}/3600 + \left(ele_{gt\_i} * R_{\text{gt}} + heat_{gb\_i} * R_{\text{gb}} + cold_{ec\_i} * R_{\text{ec}} + cold_{ac\_i} * R_{\text{ac}} + heat_{b\_i} * R_{\text{b}}\right) * Ts/3600 \right] \tag{12}$$

where $COS\,T_{\text{gas}}$, $COS\,T_{\text{ele}}$, $COS\,T_{\text{om}}$ are total natural gas cost, grid electricity cost, equipment O&M cost, respectively, $; Ts is the sampling time, s; ρ_{gas} is the density of natural gas, taken as 0.7174 kg/m^3 in this study; and C_{gas} is the unit price of natural gas, $/m^3. At the ith time step within the prediction domain, gas_{gt_i} and gas_{gb_i} represent the natural gas flow rates of the gas turbine and the gas boiler, respectively, kg/s; ele_{ec_i}, ele_{grid_i}, ele_{gt_i}, are the power of the electric chiller, the power grid, the gas turbine, respectively, kW; $heat_{b\_i}$ and $heat_{gb\_i}$ are thermal energy of the waste heat boiler and the gas boiler, kW; $cold_{ec\_i}$ and $cold_{ac\_i}$ denote cooling energy from the absorption chiller and electric chiller, kW; R_{ele_i} is grid electricity tariff, yuan/kWh. R_{gt}, R_{gb}, R_{ec}, R_{ac}, R_{b} are the O&M costs for the gas turbine, gas boiler, electric chiller, absorption chiller, and waste heat boiler, respectively, RMB/kWh.

4.3. Optimization algorithms

In this study, the load distribution rationality and real-time control effectiveness in the operation process of the IES are comprehensively considered. To achieve this, a multi-objective optimization function J is constructed by taking a weighted sum of objectives J_c and J_y:

$$J(Z_k) = w_y J_y(Z_k) + w_c J_c(Z_k) \tag{13}$$

Where w_y and w_c denote real-time control target weights and operating cost target weights, respectively.

The core objective of the optimization problem is to determine, at a specific time instance, the optimal sequence of control input commands Z_k based on the forecasted heating, cooling, and electric load. Accordingly, this goal is achieved by minimizing the objective function J, which is directly related to Z_k, leading to a tradeoff between real-time control performance and the load optimization distribution.

To achieve operational optimization and efficient control of the IES, a set of constraints is formulated for the input-output data, input increments, and waste heat distribution (between the absorption chiller and the waste heat boiler). The constraints of the input and output of each device are as follows:

$$\begin{aligned} &z_{j,\min}(i) \le z_j(k+i-1|k) \le z_{j,\max}(i) \quad i=1,2,...,p, j=1,2,...,n_z \\ &y_{j,\min}(i) - \varepsilon_k V^y_{j,\min} \le y_j(k+i|k) \le y_{j,\max}(i) + \varepsilon_k V^y_{j,\max} \quad i=1,2,...,p, j=1,2,...,n_y \end{aligned} \tag{14}$$

Where n_z represents the number of input variables; n_y denotes the number of output variables. At the ith time instant, $z_{j,\min}(i)$ and $z_{j,\max}(i)$ are the lower and upper bounds of the jth input variables; $y_{j,\min}(i)$ and $y_{j,\max}(i)$ represent the lower and upper bounds of the jth output variable. ε_k is the slack variable. V^y_j denotes the optimization weighting coefficient utilized to weaken the output constraints; typically, V^y_j takes non-negative values, and a larger value of V^y_j indicates a more lenient constraint. When the coefficient is zero, the constraint is considered a hard constraint, and any violation is not permitted.

Additionally, to mitigate the impact of significant changes in input data on the system operation, input increment constraints are introduced to impose limitations. The input increment constraints can be expressed as follows:

$$\Delta z_{j,\min}(i) \le \Delta z_j(k+i-1|k) \le \Delta z_{j,\max}(i) \quad i=1,2,...,p, j=1,2,...,n_z \tag{15}$$

Where $\Delta z_{j,\min}(i)$ and $\Delta z_{j,\max}(i)$ represent the minimum and maximum increment of the jth input variable at the ith time instant. $\Delta z_j(k+i-1|k)$ denotes the increment of the jth input variable at the ith time instant (predicted at time k).

Furthermore, considering the utilization of waste energy from the gas turbine exhaust by the absorption chiller and waste heat boiler, the waste heat allocation constraint is represented as follows:

$$q_{ex\_ac} + q_{ex\_b} \le q_{ex} \tag{16}$$

Where q_{ex_ac} and q_{ex_b} denote the waste heat utilized by the absorption chiller and the waste heat boiler, kW; and q_{ex} is the total waste heat out of the gas turbine, kW.

Due to the nonlinear characteristics of the LPV model, changes in the operational conditions of the equipment lead to variations in the model parameters. As a result, both the objective function and the constraint conditions involve nonlinear expressions of the decision variables Z_k. Consequently, the operational optimization and control process is equivalent to a nonlinear optimization problem, which can be formulated in the unified form as shown in Equation (17).

$$\begin{aligned} &\min_{Z_k} f(Z_k) \\ &\text{s.t.} \quad G_i(Z_k) = 0 \quad i=1,2,...,m_e \\ &\quad\ G_i(Z_k) \le 0 \quad i=m_e+1,...,m \end{aligned} \tag{17}$$

Where G_i represents a set of m equality and inequality constraints, and among all the constraint conditions, at least one non-linear constraint relationship exists. The function $f(Z_k)$ denotes the objective function, which is a non-linear expression of the decision variables Z_k.

Due to the simultaneous consideration of real-time control and optimal load distribution of the IES within the optimization objective function, the optimization process in this study may become more complex. To address this challenge, the Lagrange method is applied to transform such optimization problems into conventional quadratic programming problems, as reported in the literature [37]. The Sequential Quadratic Programming (SQP) algorithm is employed to solve this transformed problem. The flowchart of the SQP algorithm can be represented as shown in Fig. 9.

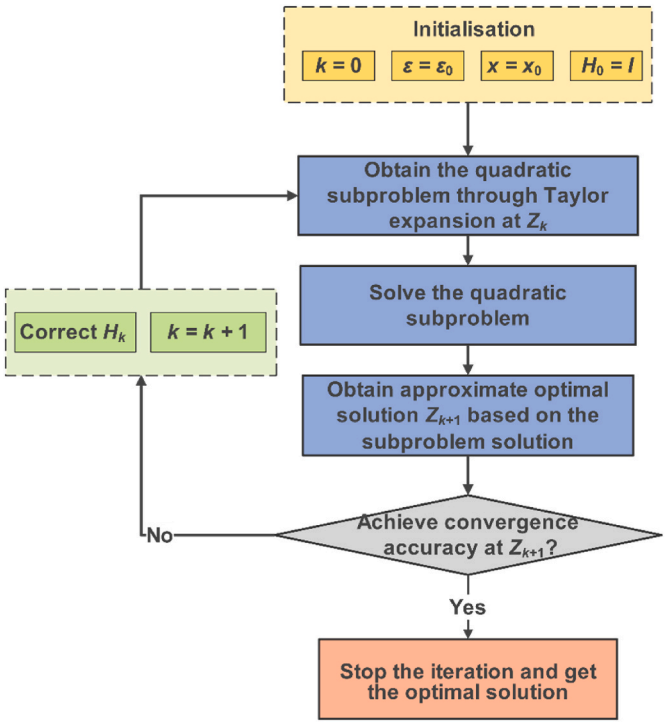

Fig. 9. Flowchart of SQP algorithm.

5. Case study

The proposed strategy is simulated in MATLAB by utilizing the NMPC toolbox based on the identified LPV models (provided in Section 3.2). The implementation of the strategy for IES based on NMPC is realized within the Simulink simulation platform, as depicted in Figure B1. Furthermore, Figure B2 illustrates the LPV models for various devices (within IES). Table 1 provides a comprehensive overview of the pertinent parameter information for the case studies, encompassing operational cost-related factors such as grid electricity tariff, natural gas price, O&M costs, equipment capacity, and those in the literature [38]. Figure C1 demonstrates the time-of-use grid electricity tariff, comprising peak, flat, and valley electricity charge rates.

5.1. Case description

To simultaneously examine the feasibility and effectiveness of the proposed strategy (also called nonlinear dynamic strategy), two cases are investigated for comparison purposes, including steady-state optimization strategy and linear dynamic optimization strategy. Table 2 presents the description of the three cases in detail. For the following comparison, a historical 24-h demand data for electricity, cooling, and heating was selected for the case study, which is presented in Fig. 10.

In the steady-state strategy, the objective function (determined as Equation (12) in Section 4.2) is formulated as the operational cost Jc of the system over the forecasting horizon, which is subject to several constraints (defined as Equation (18)), including device steady-state model constraints, bounds on various input-output variables, waste

Table 1
The pertinent parameter information for the case study [38].

Item	Value	Unit
Peak tariff $P_{grid,p}$	1.1636	RMB/kWh
Flat tariff $P_{grid,f}$	0.8656	RMB/kWh
Valley tariff $P_{grid,v}$	0.3536	RMB/kWh
Natural gas price C_{gas}	2.8	RMB/m^3
Gas turbine O&M cost R_{gt}	0.03	RMB/kWh
Waste heat boiler O&M cost R_b	0.012	RMB/kWh
Gas boiler O&M cost R_{gb}	0.015	RMB/kWh
Absorption chiller O&M cost R_{ac}	0.025	RMB/kWh
Electric chiller O&M cost R_{ec}	0.01	RMB/kWh
Rated capacity of gas turbine $ele_{gt,max}$	6000	kW
Rated capacity of absorption chiller $cold_{ac,max}$	9200	kW
Rated heat supply of waste heat boiler $heat_{b,max}$	3500	kW
Rated refrigeration capacity of electric chiller $cold_{ec,max}$	14000	kW
Rated heating capacity of gas boiler $heat_{gb,max}$	2500	kW

Table 2
Description of three cases.

Case	Description
Proposed strategy (NL-dynamic strategy)	Based on the LPV model (considering the nonlinear dynamic model), the proposed strategy by utilizing NMPC is formulated for IES.
Steady-state optimization strategy (Steady-state strategy)	Based on the steady-state model, the steady-state optimization strategy is established for IES by using the dispatching optimization method.
Linear dynamic optimization strategy (L-dynamic strategy)	Based on the linear dynamic system model, the linear dynamic optimization strategy by using linear MPC is conducted for IES.

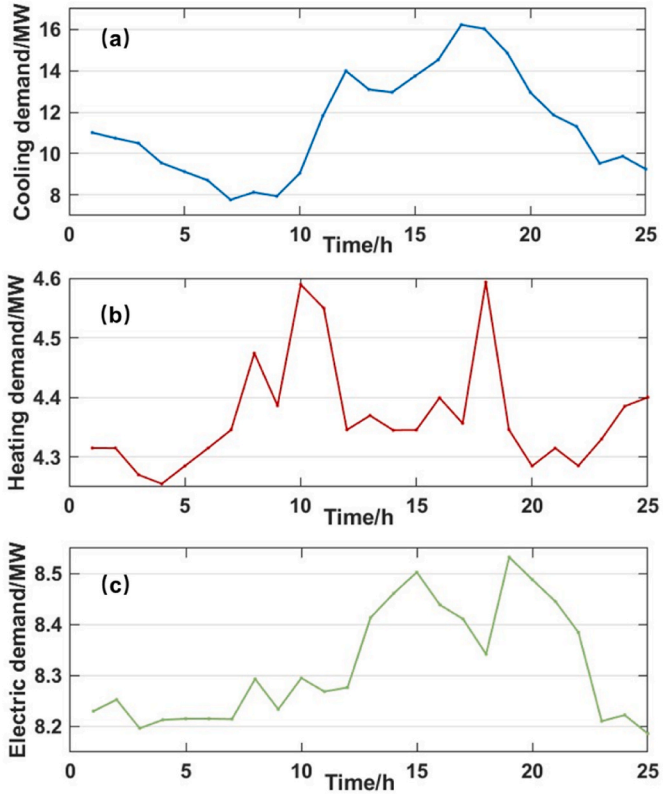

Fig. 10. (a) Selected 24-h cooling demand profile. (b) Selected 24-h heating demand profile. (c) Selected 24-h electric demand profile.

heat distribution constraints, and supply-demand balance constraints.

$$\begin{cases} ele_{gt} = -1137 v_{gt}^{-0.5809} + 7307 \\ q_{ex} = -698.2 v_{gt}^{-0.6912} + 9835 \\ heat_b = -0.3 a_b^2 + 99.6 a_b - 2902.9 \\ heat_{gb} = -2417.3 v_{gb}^2 + 4842.2 v_{gb} + 120.0 \\ cold_{ac} = -2.5 a_{ac}^2 + 467.8 a_{ac} - 13243.8 \\ cold_{ec} = -6.1 ele_{ec} - 04 ele_{ec}^2 + 8.8 ele_{ec} - 8433.1 \\ z_{j_1,\min}(i) \le z_{j_1}(k+i-1|k) \le z_{j_1,\max}(i) \\ y_{j_2,\min}(i) \le y_{j_2}(k+i|k) \le y_{j_2,\max}(i) \\ q_{ex\_ac}(k+i|k) + q_{ex\_b}(k+i|k) \le q_{ex}(k+i|k) \\ \sum_{cold} y(k+i|k) = Q_{cold}(k+i|k), \sum_{heat} y(k+i|k) = Q_{heat}(k+i|k) \end{cases} \quad \begin{matrix} i = 1,2,\ldots,p \\ j_1 = 1,2,\ldots,n_z \\ j_2 = 1,2,\ldots,n_y \end{matrix} \tag{18}$$

Where ele_{gt} and q_{ex} are power supply and waste heat of gas turbine, respectively; v_{gt} is the extent of the valve opening of gas turbine; $heat_b$ is heat supply of waste heat boiler; a_b is the damper angle of the induced draft fan of waste heat boiler; $heat_{gb}$ is heat supply of gas boiler; v_{gb} is the extent of the valve opening of gas boiler; $cold_{ac}$ is cooling output of absorption chiller; a_{ac} is damper angle of the induced draft fan of absorption chiller; $cold_{ec}$ is cooling output of electric chiller; ele_{ec} is input power of electric chiller; $\sum_{cold} y(k+i|k)$ and $\sum_{heat} y(k+i|k)$ represent the summation of cooling and heating outputs from all cooling and heating devices at time k for the predicted time step $k + i$, *respectively;* $Q_{cold}(k+i|k)$ and $Q_{heat}(k+i|k)$ represent the cooling and heating demand at time k for the predicted time step $k + i$, *respectively*. The meanings of the remaining variables are reported in Section 4.

In the L-dynamic strategy, the operational optimization employs the MPC-based rolling optimization mode, where the objective function is defined by the function J as formulated in Equation (13). The constraint conditions align with those defined in Section 4.3. Besides, the linear dynamic models of various devices, which are employed in L-dynamic strategy, are delineated as follows:

$$\begin{cases} ELE_{gt} = \dfrac{84.5s + 542.4}{s^2 + 0.7218s + 0.3462} V_{gt} \\ HEAT_b = \dfrac{1.486s + 0.01217}{s^2 + 0.04169s + 0.0002137} A_b \\ HEAT_{gb} = \dfrac{302.5s + 14.26}{s^2 + 0.2121s + 0.005829} V_{gb} \\ COLD_{ac} = \dfrac{0.437}{s + 0.003718} A_{ac} \\ COLD_{ec} = \dfrac{0.6161}{s + 0.0102} ELE_{ec} \end{cases} \tag{19}$$

Where ELE_{gt}, V_{gt}, $HEAT_b$, A_b, $HEAT_{gb}$, V_{gb}, $COLD_{ac}$, A_{ac}, $COLD_{ec}$, and ELE_{ec} are the Laplace transform of ele_{gt}, v_{gt}, $heat_b$, a_b, $heat_{gb}$, v_{gb}, $cold_{ac}$, a_{ac}, $cold_{ec}$, and ele_{ec}, respectively.

5.2. Supply-demand balance performance

In order to investigate the dynamic performance and load distribution effect of NL-dynamic strategy, a typical hierarchical strategy (steady-state strategy) utilizing steady-state models is developed for comparison. In the steady-state strategy, the obtained scheduling instructions, which are derived from the optimization results in the scheduling layer, is sent to the control layer for tracking the scheduling plan. However, since the lack of dynamic characteristics for the devices and pipeline networks during optimization, the scheduling instructions obtained from steady-state optimization results may fail to ensure real-

time supply-demand balance, leading to an uneven load distribution over cooling, heating, and electric demand.

Fig. 11 (a) describes that the electricity output (in both NL-dynamic strategy and steady-state strategy) is temporally matched to the electric demand, which is because the equipment (within IES) can respond quickly to electric demand. In the NL-dynamic strategy, the heating and cooling output is balanced with the heating and cooling demand (i.e., the blue histogram is not matched to the dotted line). However, owing to the heating and cooling supply delay, there are noticeable deviations between the actual cooling and heating supply in the steady-state strategy and the 24-h cooling and heating demand (i.e., the blue histogram is not matched to the dotted line), as indicated in Fig. 11(b) and (c).

To quantify the quantitative effectiveness of load distribution, the average deviation of supply and demand balance (namely the average supply-demand deviation index) is defined as Equation (20). The simulation scenarios have 24-h spans with a sampling time of 15 min, resulting in a total of 97 sampling instances. For the NL-dynamic strategy, the average supply-demand deviation index for cooling is calculated to be 1.64 %, and for heating, it is 0.94 %. In contrast, for the

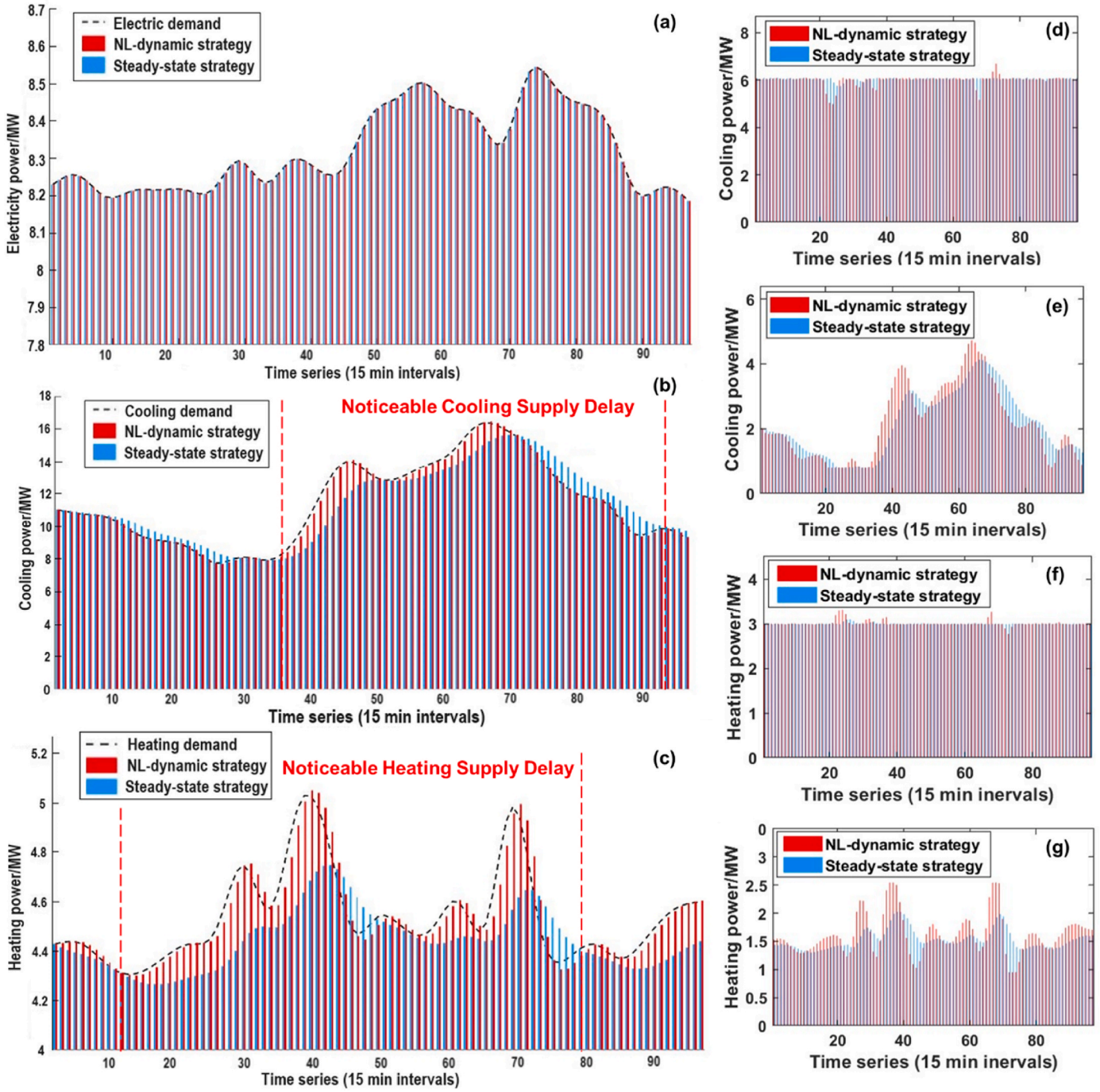

Fig. 11. (a) Comparison between simulation results and electricity demand. (b) Comparison between simulation results and cooling demand. (c) Comparison between simulation results and heating demand. (d) Comparison of cooling power of absorption chiller between the steady-state strategy and the NL-dynamic strategy. (e) Comparison of cooling power of electric chiller between the steady-state strategy and the NL-dynamic strategy. (f) Comparison of heating power of waste heat boiler between the NL-dynamic strategy and the steady-state strategy. (g) Comparison of heating power of gas boiler between the NL-dynamic strategy and the steady-state strategy.

steady-state strategy, the average supply-demand deviation index for cooling is calculated to be 6.75 %, and for heating, it is 2.71 %. Comparatively, the average supply-demand deviation for cooling and heating in the steady-state strategy is approximately 3–4 times larger than that in the NL-dynamic strategy. The observed phenomenon can be attributed to the significant thermal inertia in the cooling and heating supply processes compared to the electricity supply process, especially evident in the cooling and heating networks. Due to pipe network length and system thermal capacity, the cooling and heating supply processes require a certain amount of time. In the steady-state strategy, the optimization calculation is based on the steady-state model of the system, neglecting the time required for energy transmission in the cooling and heating supply processes. As a result, the cooling and heating supply may not be delivered promptly to meet the end-user demand. It is caused by the simplified approach in the steady-state strategy, where dynamic characteristics related to energy transmission are not considered in the optimization process.

$$KPI_{\mathrm{Cold}} = \frac{\sum_{i=1}^{97} \frac{\left|cold_{\mathrm{sys}}(i) - Q_{\mathrm{Cold}}(i)\right|}{Q_{\mathrm{Cold}}(i)}}{97}$$
$$KPI_{\mathrm{Heat}} = \frac{\sum_{i=1}^{97} \frac{\left|heat_{\mathrm{sys}}(i) - Q_{\mathrm{Heat}}(i)\right|}{Q_{\mathrm{Heat}}(i)}}{97} \tag{20}$$

To further verify the impact of thermal inertia in heating and cooling supply processes, comparative analyses of heating and cooling supply of devices (over 24 h) are conducted, the details of which are introduced from Fig. 11 (d) to Fig. 11 (g). During periods of pronounced fluctuations in demand, proper adjustments in the energy supply (for various devices) are crucial to obtain an optimal load distribution scheme, leading to an excellent dispatch. Based on the 24-h demand profile referenced in Fig. 10, noticeable local peaks in cooling demand are observed around the 45th and 67th time steps, while local peaks in heating demand occur around the 28th, 38th, 50th, 60th, and 70th time steps. In both strategies, the primary schemes of adjusting the cooling and heating supply are through the electric chiller and gas boiler. By employing a steady-state model, the energy supply of main devices in the steady-state strategy precisely aligns with the corresponding demand peaks. Considering the dynamic characteristics of IES, the energy supply of main devices in the NL-dynamic strategy precedes the demand peaks by 2∼3 time steps, approximately 30 min–45 min in advance. Additionally, the energy supply of the devices in the NL-dynamic strategy demonstrates higher local peaks compared to the steady-state strategy. By accounting for the dynamic characteristics of the IES, the NL-dynamic strategy exhibits a more accurate and efficient load distribution, leading to improved supply-demand balance during periods of substantial demand fluctuations. Thus, compared with energy management, which only considers steady-state characteristics, the deviations between actual equipment output and optimal energy management tasks can be mitigated by using the LPV model.

Comparing the results of the heating supply of the waste heat boiler in Fig. 11 (f), it is evident that the NL-dynamic strategy shows a significantly higher heating capacity than the steady-state strategy around the 25th, 32nd, 36th, and 67th time steps. It reveals that during rapid demand growth periods, the increment in the heating supply of the gas boiler would result in the actual heating capacity of IES being unable to keep up with heating demand. As demonstrated in the NL-dynamic strategy, this approach illustrates the importance of considering the dynamic characteristics of the IES, which ultimately achieves a superior load distribution.

5.3. Economic performance

When addressing the limitations of steady-state strategy, a linear dynamic strategy (L-dynamic strategy) by incorporating an approximate-linear or piecewise-linear dynamic model is utilized to enhance optimization effects considering system dynamics (see Equation (20)). Although the L-dynamic strategy exhibits a pretty good computational efficiency, the pronounced deviation between the simulation result (obtained from linear dynamic strategy) and the characteristics of the actual operation is found. To explore the operational economic performance of IES with consideration of nonlinearities, the L-dynamic strategy is propounded in comparison to the NL-dynamic strategy.

Fig. 12 illustrates the comparison between simulation results (of L-dynamic strategy) and selected 24-h demands (reported in Fig. 10). Overall, the simulation results suggest that despite neglecting the system's nonlinearity, the energy supply in the L-dynamic strategy (including cooling, heating, and electricity) can maintain a basic balance with demands (displaying reasonable load distribution). It is caused by accurate tracking derived from the control layer and assuming a centralized mass regulation mode for the pipe networks, where the flow rate and heat loss remain relatively constant, leading to the pipe networks having a pretty well-linear characteristic [39].

The load distribution scheme of various devices in the IES is diverse and complex. In the power supply stage, there exist various approaches for distributing power between the gas turbine and the external power grid. In the heating and cooling supply section, the allocation of waste heat from the gas turbine exhibits variability. Due to the non-linear characteristics of the devices, the economic performance of the energy supply of devices may change under different operational conditions. As a result, real-time adjustments are necessitated by the load distribution scheme to ensure optimal economic revenue. From Fig. 13 (a)–13 (f) compare the load distribution scheme of each operating device in the NL-dynamic strategy and the L-dynamic strategy.

The results of the comparative analysis of the cumulative operational costs for the 24-h operation (of the IES) in the NL-dynamic strategy and the L-dynamic strategy are presented in Fig. 13 (g) and Table 3. Fig. 13 (g) depicts a comparative analysis of the cumulative operating costs between the NL-dynamic strategy and the L-dynamic strategy. While both cases achieve optimal load distribution in the IES, the NL-dynamic strategy consistently maintains lower cumulative operational costs throughout the operational optimization process. As the operating time increases, the difference in cumulative operational costs between the two strategies becomes more significant, indicating that the NL-dynamic strategy can achieve a more economically reasonable operational scheme in each optimization and control cycle. The 24-h total cost for the NL-dynamic strategy is 163,899 RMB, while for the L-dynamic strategy, it is 195,063 RMB. Compared to the L-dynamic strategy, which neglects the overall nonlinear characteristics of the IES, the NL-dynamic strategy, considering nonlinear dynamic characteristics, manages to reduce operational costs by 16 %, with a slightly increased optimization solving time. However, this minor computational burden is deemed acceptable in light of the economic benefits obtained.

6. Conclusions

To enhance equipment output performance and operational economic benefit, we proposed an NMPC-based optimal load distribution and real-time control strategy for IES, including the LPV model under varying operational conditions, the real-time prediction objective, and the optimal load distribution objective. Then, the steady-state strategy and the L-dynamic strategy are designed for the case study to investigate the supply-demand balance and economic performance of the proposed strategy. Several meaningful conclusions can be drawn.

(1) The developed LPV models for various devices consistently maintain high accuracy even under varying operational conditions, effectively capturing the dynamic behaviors and nonlinear behaviors inherent to device operation. Moreover, the formulated network models for the cooling and heating supply process are

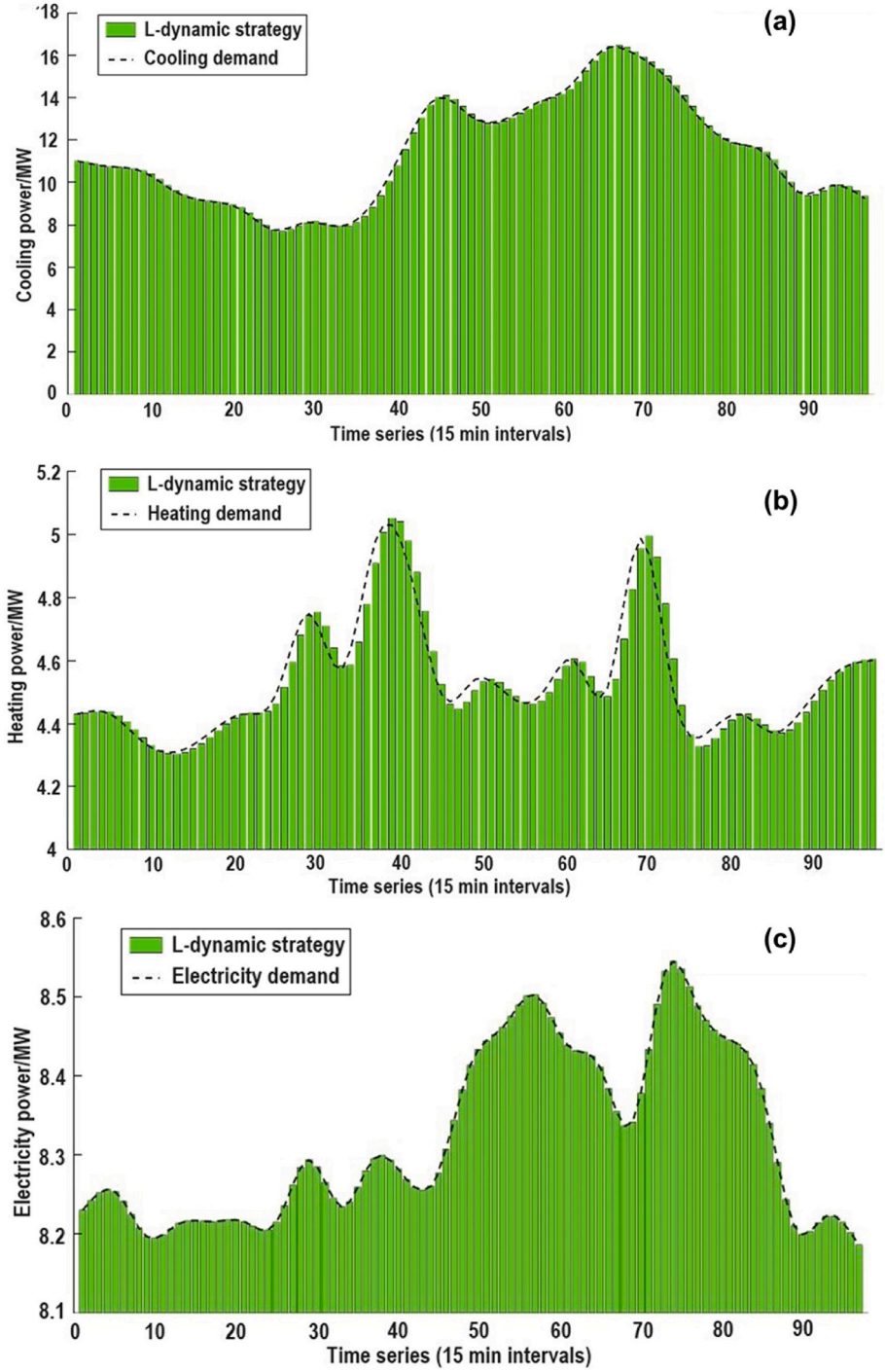

Fig. 12. (a) Comparison between simulation result of L-dynamic strategy and 24-h cooling demand. (b) Comparison between simulation result of L-dynamic strategy and 24-h heating demand. (c) Comparison between simulation result of L-dynamic strategy and 24-h electricity demand.

applied to characterize the intricate energy transportation dynamics intrinsic to the simulation system.

(2) Compared with the steady-state strategy, the proposed strategy is used to avoid energy supply delays. As a consequence, the average energy supply-demand deviation of the proposed strategy (for cooling and heating) is about 1/4∼1/3 times that of the steady-state strategy. By employing the proposed strategy, an optimal load distribution of cooling, heating, and electricity can be achieved, leading to an improvement in equipment output performance.

(3) In contrast to the L-dynamic strategy, the proposed strategy, which fully considers the nonlinear characteristics of devices, can accurately model the input-output relationships of devices and effectively avoid untimely equipment output. Consequently, the cost-efficient scheduling scheme is formulated, effectively reducing the operational costs of the IES. Through the case study, the proposed strategy demonstrates a 16 % reduction in operation cost compared with the L-dynamic optimization strategy.

In the future, it is expected to further investigate how to tune different prediction horizons for different variables, to maximize control

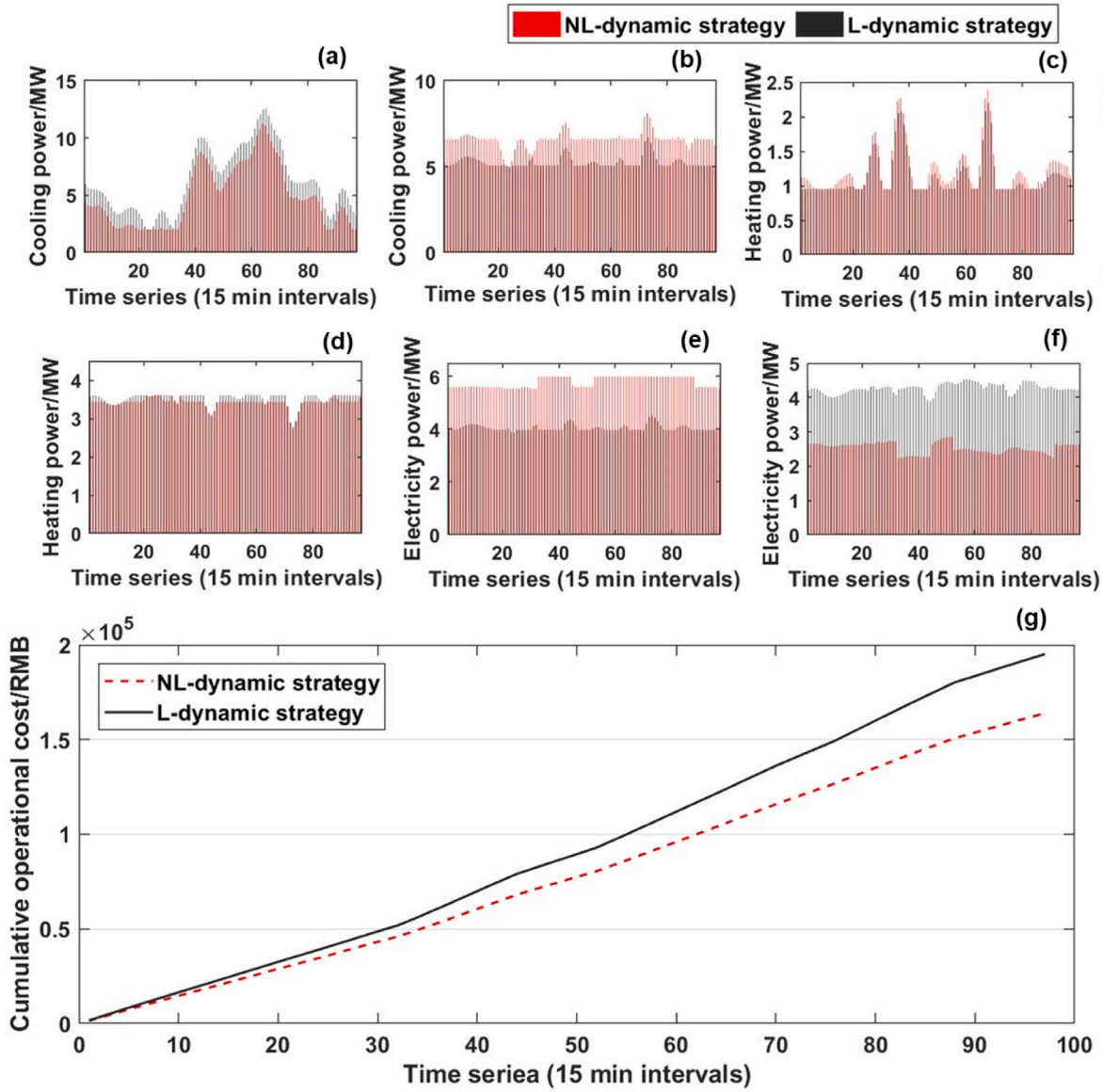

Fig. 13. (a) Comparison of load distribution scheme of electric chiller. (b) Comparison of load distribution scheme of absorption chiller. (c) Comparison of load distribution scheme of gas boiler. (d) Comparison of load distribution scheme of waste heat boiler. (e) Comparison of load distribution scheme of gas turbine. (f) Comparison of load distribution scheme of external power grid. (g) Comparison of cumulative operational costs.

Table 3
Comparison of simulation results between the NL-dynamic strategy and the L-dynamic strategy.

Item	24-h actual total operational cost (RMB)	Simulation solving time (sec)
NL-dynamic strategy	163899	58
L-dynamic strategy	195063	42

performance of the MIMO MPC.

CRediT authorship contribution statement

Jiarui Li: Writing – original draft, Visualization, Methodology, Investigation, Formal analysis. **Zhiwei Jiang:** Writing – original draft, Visualization, Methodology, Investigation, Conceptualization. **Yuan Zhao:** Project administration, Investigation, Data curation. **Xiaolu Feng:** Writing – review & editing, Supervision, Project administration, Methodology, Investigation. **Menglian Zheng:** Writing – review & editing, Supervision, Project administration, Investigation.

Declaration of competing interest

The authors declare that they have no known competing financial interests or personal relationships that could have appeared to influence the work reported in this paper.

Data availability

Data will be made available on request.

Acknowledgements

This work was supported by the Fundamental Research Funds for the Central Universities [grant number 2022ZFJH004].

Appendix D. Supplementary data

Supplementary data to this article can be found online at https://doi.org/10.1016/j.energy.2024.132878.

Appendix A. APROS-based Model

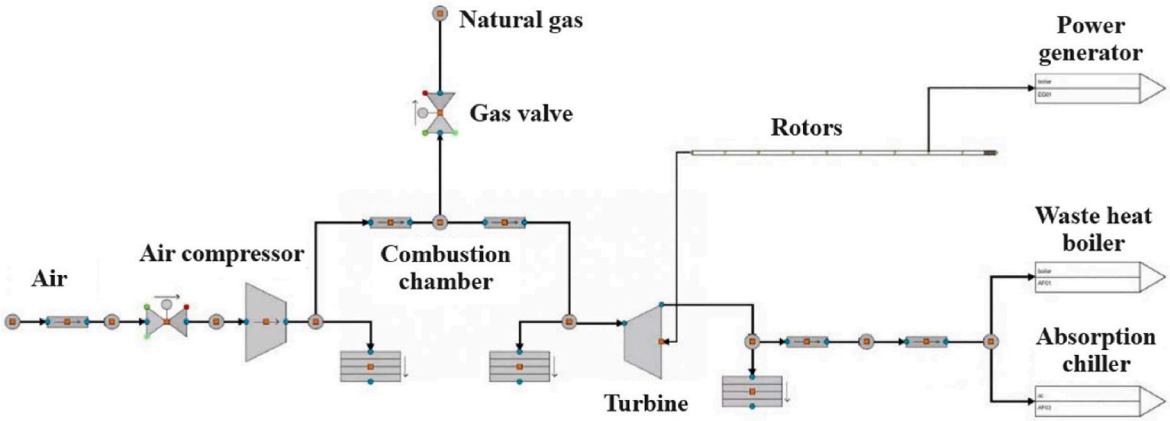

Fig. A1. Gas turbine simulation system.

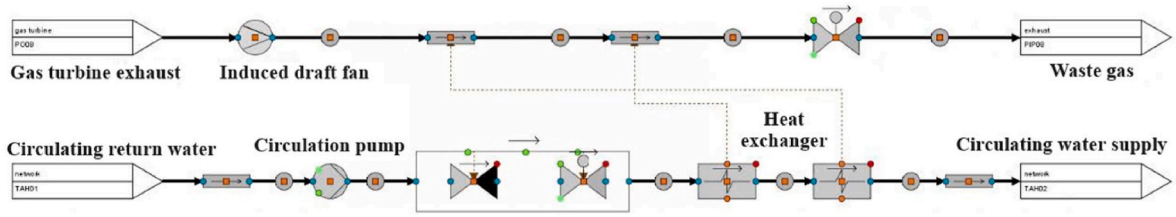

Fig. A2. Waste heat boiler simulation system.

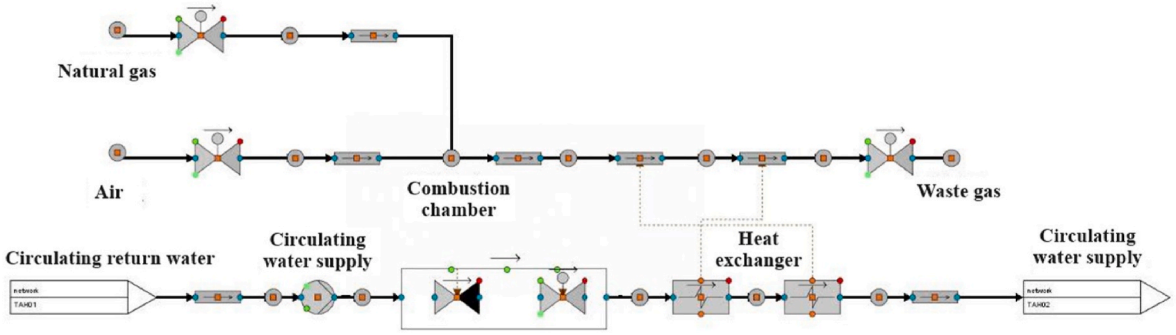

Fig. A3. Gas boiler simulation system.

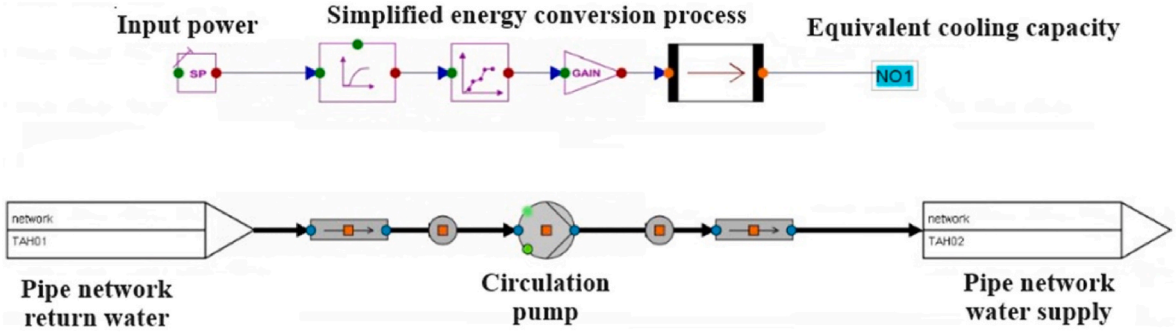

Fig. A4. Electric chiller simulation system.

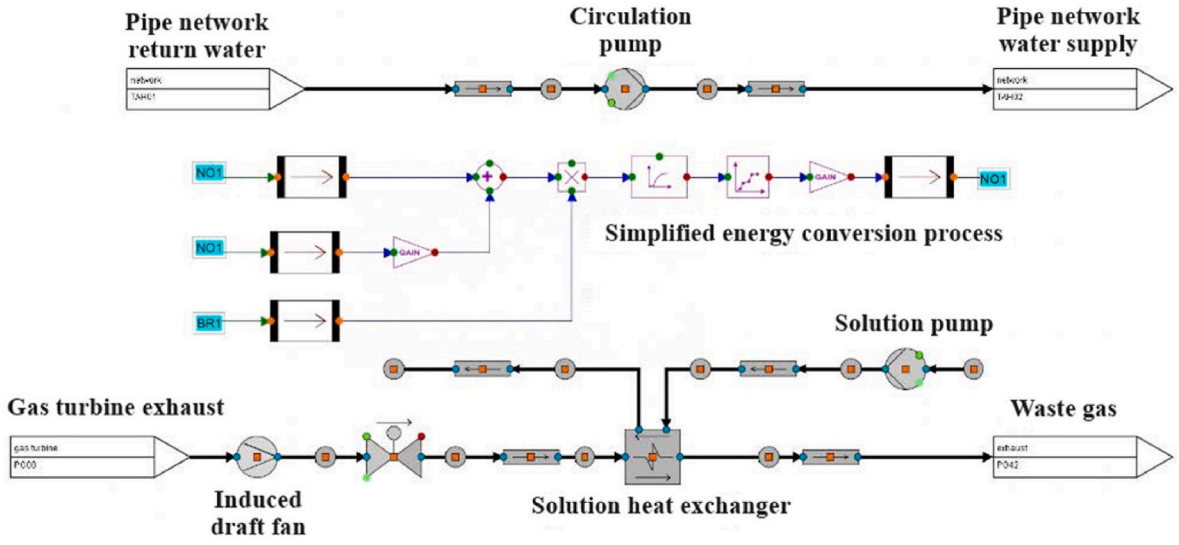

Fig. A5. Absorption chiller simulation system.

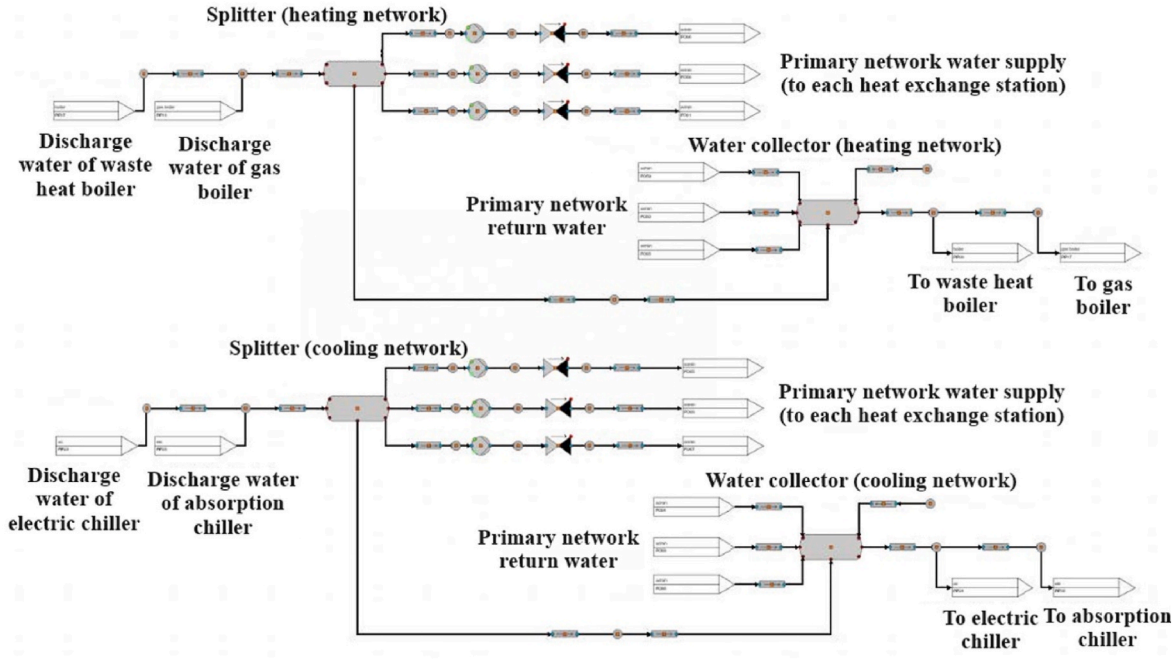

(a) Primary network

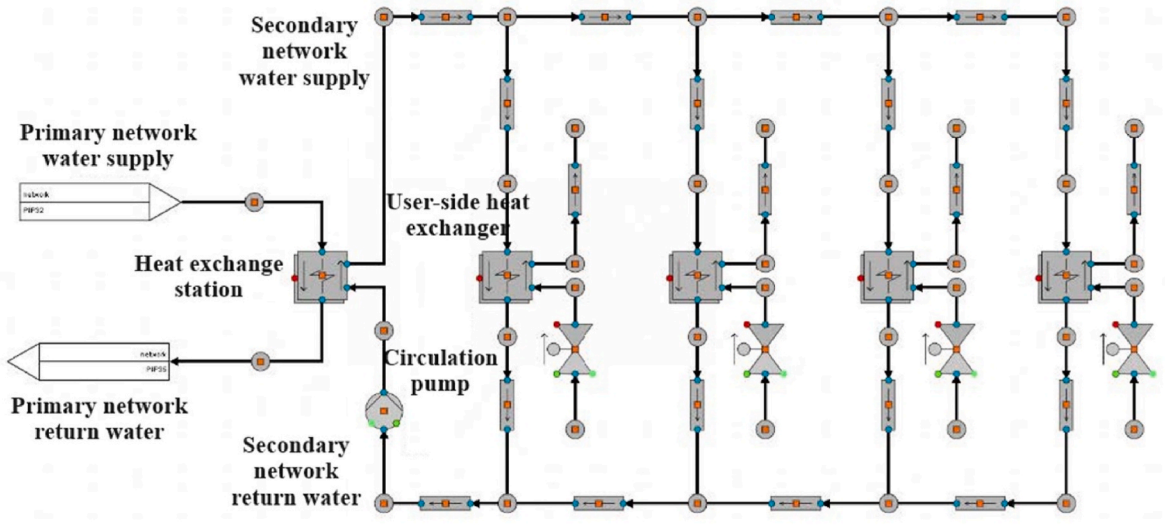

(b) Secondary network

Fig. A6. Pipe network simulation system
(a) Primary network
(b) Secondary network.

Appendix B. Simulation model

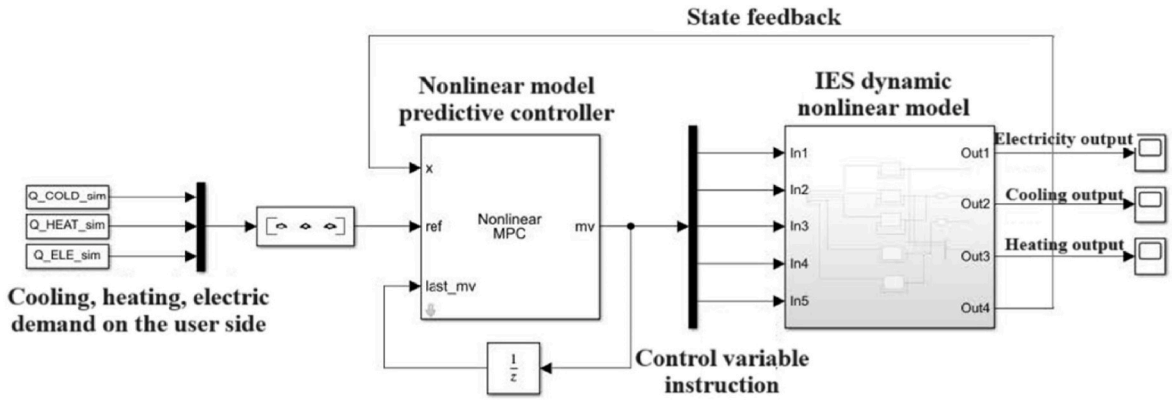

Fig. B1. NMPC-based optimal load distribution and real-time control model for IES.

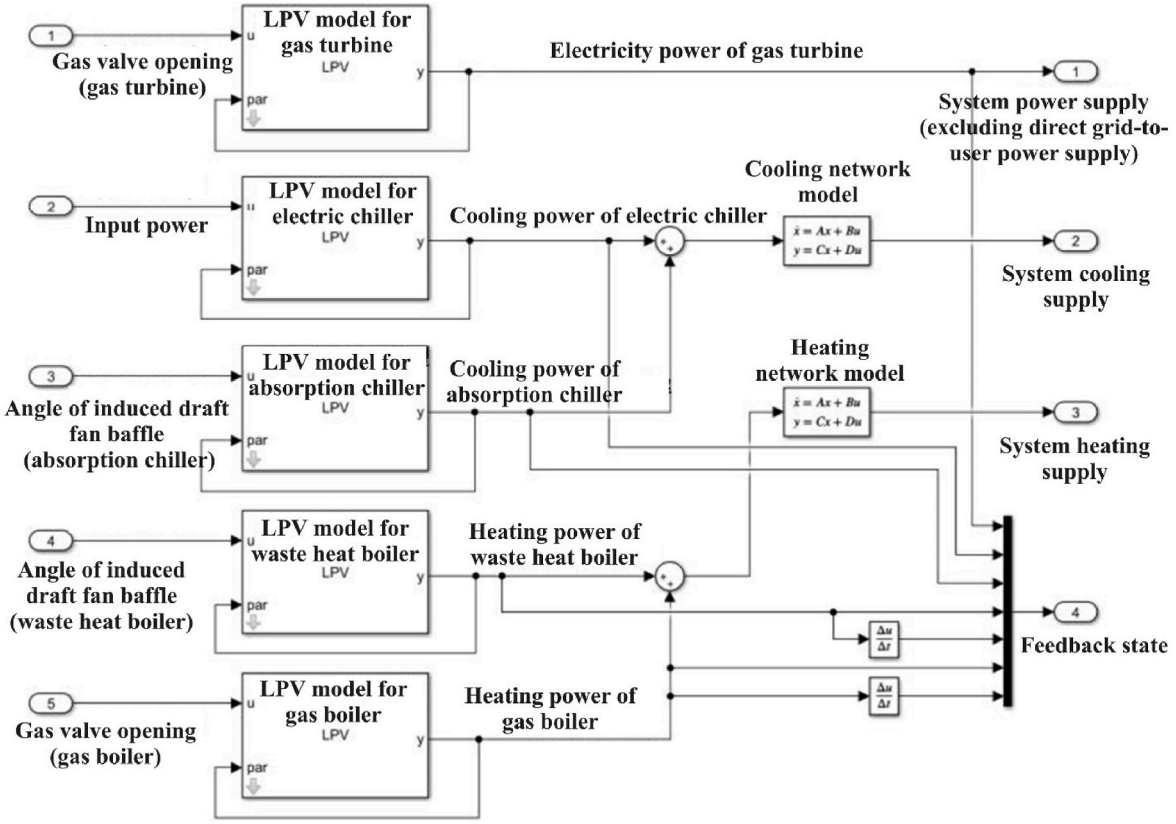

Fig. B2. IES dynamic nonlinear model.

Appendix C. The time-of-use grid electricity tariff of case studies

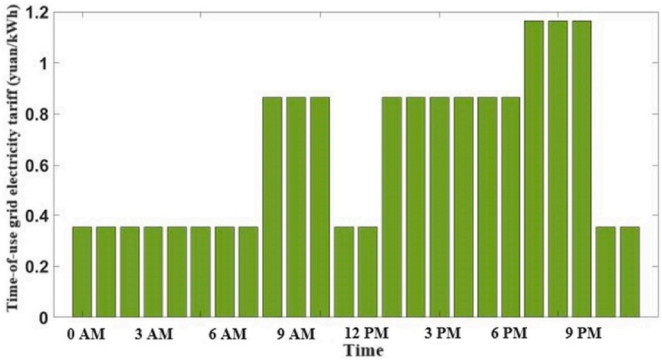

Fig. C1. Time-of-use grid electricity tariff of case studies.

References

[1] Xue L, Wang J, Zhang Y, et al. Model-data-event based community integrated energy system low-carbon economic scheduling. Renew Sustain Energy Rev 2023; 182:113379.
[2] Zhu Y, Xu Y, Chen H, et al. Optimal dispatch of a novel integrated energy system combined with multi-output organic Rankine cycle and hybrid energy storage. Appl Energy 2023;343:121113.
[3] Liu C, Wang C, Yin Y, et al. Bi-level dispatch and control strategy based on model predictive control for community integrated energy system considering dynamic response performance. Appl Energy 2022;310:118641.
[4] Wang Yu, Ke LI, Shuzhen LI, et al. A bi-level scheduling strategy for integrated energy systems considering integrated demand response and energy storage co-optimization. J Energy Storage 2023;66:107508.
[5] Basu M. Optimum dynamic dispatch of clean water, methane, electricity and heat considering carbon capture. J Clean Prod 2024;435:140451.
[6] Bu F, Wang S, Bai H, et al. An integrated demand response dispatch strategy for low-carbon energy supply park considering electricity–hydrogen–carbon coordination. Energy Rep 2023;9:1092–101.
[7] Wang J, Mao J, Hao R, et al. Multi-energy coupling analysis and optimal scheduling of regional integrated energy system. Energy 2022;254:124482.
[8] Nazir MS, Almasoudi FM, Abdalla AN, et al. Multi-objective optimal dispatching of combined cooling, heating and power using hybrid gravitational search algorithm and random forest regression: towards the microgrid orientation. Energy Rep 2023; 9:1926–36.
[9] Xu J, Gao C, Yan Z, et al. Low carbon optimal operation of integrated energy systems considering air pollution emissions. Energy Rep 2023;9:1597–606.
[10] Chen J, Chen H, Lin Z, et al. Multi-objective optimal dispatch of integrated heat and electricity energy systems considering heat load energy quality. Energy Rep 2023;9:1191–200.
[11] Yao L, Liu Z, Chang W, et al. Multi-level model predictive control based multi-objective optimal energy management of integrated energy systems considering uncertainty. Renew Energy 2023;212:523–37.
[12] Zhao Y, Li Z, Ju P, et al. Two-stage data-driven dispatch for integrated power and natural gas systems by using stochastic model predictive control. Appl Energy 2023;343:121201.
[13] Majji RK, Mishra JP, Dongre AA. Model predictive control based autonomous DC microgrid integrated with solar photovoltaic system and composite energy storage. Sustain Energy Technol Assessments 2022;54:102862.
[14] Turk A, Wu Q, Zhang M. Model predictive control based real-time scheduling for balancing multiple uncertainties in integrated energy system with power-to-x. Int J Electr Power Energy Syst 2021;130:107015.
[15] Liu C, Wang C, Yin Y, et al. Bi-level dispatch and control strategy based on model predictive control for community integrated energy system considering dynamic response performance. Appl Energy 2022;310:118641.
[16] Yu Y, Li J, Chen D. Optimal dispatching method for integrated energy system based on robust economic model predictive control considering source–load power interval prediction. Global Energy Interconnection 2022;5:564–78.
[17] Wanjiru EM, Sichilalu SM, Xia X. Model predictive control of heat pump water heater-instantaneous shower powered with integrated renewable-grid energy systems. Appl Energy 2017;204:1333–46.
[18] Wei S, Gao X, Zhang Y, et al. An improved stochastic model predictive control operation strategy of integrated energy system based on a single-layer multi-timescale framework. Energy 2021;235:121320.
[19] Wu L, Yin X, Pan L, et al. Economic model predictive control of integrated energy systems: a multi-time-scale framework. Appl Energy 2022;328:120187.
[20] Yang C, Zhu Y, Zhou J, et al. Dynamic flexibility optimization of integrated energy system based on two-timescale model predictive control. Energy 2023;276: 127501.
[21] Hu K, Wang B, Cao S, et al. A novel model predictive control strategy for multi-time scale optimal scheduling of integrated energy system. Energy Rep 2022;8:7420–33.
[22] Zhu J, Cui X, Ni W. Model predictive control based control strategy for battery energy storage system integrated power plant meeting deep load peak shaving demand. J Energy Storage 2022;46:103811.
[23] Jin Y, Wu X, Shen J, et al. Distributed model predictive coordinated control for combined heat and power load of an integrated energy system. IFAC-PapersOnLine 2022;55:507–12.
[24] Wu L, Yin X, Pan L, et al. Distributed economic predictive control of integrated energy systems for enhanced synergy and grid response: a decomposition and cooperation strategy. Appl Energy 2023;349:121627.
[25] Lv C, Yu H, Li P, et al. Model predictive control based robust scheduling of community integrated energy system with operational flexibility. Appl Energy 2019;243:250–65.
[26] Köhler J, Müller MA, Allgöwer F. Analysis and design of model predictive control frameworks for dynamic operation—an overview. Annu Rev Control 2024;57: 100929.
[27] Morato MM, Normey-Rico JE, Sename O. Model predictive control design for linear parameter varying systems: a survey. Annu Rev Control 2020;49:64–80.
[28] Morato MM, Mendes PRC, Normey-Rico JE, et al. LPV-MPC fault-tolerant energy management strategy for renewable microgrids. Int J Electr Power Energy Syst 2020;117:105644.
[29] Bernardi E, Morato MM, Mendes PRC, et al. Fault-tolerant energy management for an industrial microgrid: a compact optimization method. Int J Electr Power Energy Syst 2021;124:106342.
[30] Godoy JL, Schierloh RM. Predictive management of the hybrid generation dispatch and the dispatchable demand response in microgrids with heating, ventilation, and air-conditioning (HVAC) systems. Sustainable Energy, Grids and Networks 2022; 32:100857.
[31] Li J, Wang Z, Li S, et al. A SDNN-MPC method for power distribution of COGAG propulsion system. Energy 2022;254:124310.
[32] Zhu Y, Zou J, Li S, et al. Nonlinear model predictive control of PEMFC anode hydrogen circulation system based on dynamic coupling analysis. Int J Hydrogen Energy 2023;48:2385–400.
[33] Ji G, Huang J, Zhang K, et al. Identification and predictive control for a circulation fluidized bed boiler. Knowl Base Syst 2013;45:62–75.
[34] Shi Y, Zhang Z, Chen X, et al. Data-Driven model identification and efficient MPC via quasi-linear parameter varying representation for ORC waste heat recovery system. Energy 2023;271:126959.
[35] Campus Metabolism. https://cm.asu.edu/.
[36] Zhu Y. Multivariate system identification for process control. 2005.
[37] Morato MM, Normey-Rico JE, Sename O. Model predictive control design for linear parameter varying systems: a survey. Annu Rev Control 2020;49:64–80.
[38] Zhou Y. Optimal scheduling of microgrid systems for counting and heat and humidity load response. Hangzhou, Zhejiang, China: Master Thesis) Zhejiang University; 2022.
[39] Lin XJ, Zhang N, Mao YH, et al. A review of the transformation from urban centralized heating system to integrated energy system in smart city. Appl Therm Eng 2024;240:122272.